UNLV Theses, Dissertations, Professional Papers, and Capstones

8-2012

Paleoseismic Study of the Stewart Valley and Northern Pahrump Segments of the Stateline Fault System, Nevada

Jonathan Carter
University of Nevada, Las Vegas, Carterj7@unlv.nevada.edu

Follow this and additional works at: https://digitalscholarship.unlv.edu/thesesdissertations

Part of the Geology Commons, Geophysics and Seismology Commons, and the Tectonics and Structure Commons

PALEOSEISMIC STUDY OF THE STEWART VALLEY

AND NORTHERN PAHRUMP SEGMENTS

OF THE STATELINE FAULT

SYSTEM, NEVADA

By

Jonathan A. Carter

Bachelor of Science
University of Nevada, Las Vegas
2009

A thesis submitted in partial fulfillment
of the requirements for the

Master of Science in Geoscience

Department of Geoscience
College of Sciences
Graduate College

University of Nevada, Las Vegas
August 2012

THE GRADUATE COLLEGE

We recommend the thesis prepared under our supervision by

Jonathan Carter

entitled

Paleoseismic Study of the Stewart Valley and Northern Pahrump Segments of the Stateline Fault System, Nevada

be accepted in partial fulfillment of the requirements for the degree of

Master of Science in Geoscience
Department of Geoscience

Wanda Taylor, Ph.D., Committee Chair

Brenda Buck, Ph.D., Committee Member

Michael Wells, Ph.D., Committee Member

Barbara Luke, Ph.D., Graduate College Representative

Thomas Piechota, Ph. D., Interim Vice President for Research and Graduate Studies and Dean of the Graduate College

August 2012

ABSTRACT

Paleoseismic study of the Stewart Valley and Northern Pahrump segments of the Stateline Fault System, Nevada.

By

Jonathan Carter

Dr. Wanda J. Taylor, Examination Committee Chair

Professor of Geoscience

University of Nevada, Las Vegas

The Stateline fault system (SFS) is a ~200 km long zone of dextral faults running NW along the NV/CA border from Primm, Nevada to Amargosa Valley in the western Central Basin and Range province (CBR). Because of size and proximity, the SFS poses a hazard to the 2.5 million people, most of who live within 10 km, in Pahrump, Nevada and within 40 km, in Las Vegas, Nevada. The goals of this thesis are to (1) understand if the SFS is accommodating faulting slip change in the CBR; (2) test the along strike continuity of the SFS in Pahrump and Stewart valleys; (3) establish the magnitudes, ages and frequencies of earthquakes on the SFS; and (4) better represent the potential hazard of future earthquakes.

A cross fault trench study of the SFS in Stewart Valley displays sediment horizons with offsetting fault surfaces and liquefaction. [14]C ages of samples from above and below fault tips suggest three or possibly four earthquake events. Earthquake formed bevels in fault scarp topographic profiles also support 3 or 4

possible scarp forming events having occurred on the SFS recently enough to not have been eroded away.

This research establishes the surface location and offset of the SFS in Stewart Valley and the offset and interaction of the W116F and WSMF with the SFS. The trench survey, fault scarps, and previous seismic reflection studies supports a fault continuity along-strike as the SFS extends from Pahrump Valley and into Stewart Valley. Using water well log lithologies in a 3D model a 10 km dextral offset of fine- and coarse-grained sediments in Pahrump Valley by a previously undocumented fault, the here named West 116 fault (W116F) is apparent. The SFS scarp heights and locations in the Pahrump and Stewart valleys suggest that the SFS, WSMF, and W116F interact.

Earthquakes occurring on the SFS that are >M5 have occurred in the past. This is supported by the presence of liquefaction, fault scarp formation, and both the local and overall surface rupture length of the SFS. At least three and possibly four strong earthquakes occurred on the SFS 2 in the last 3340 cal yrs B.P., inferred from fault scarp topography bevels, offsets in the trenches and relevant ^{14}C dates. Using the total surface rupture length of 200 km an estimated M7.8 earthquake could occur on the SFS. The SFS is accommodating change in the CBR between western strike-slip faults and the eastern extensional faults along the WSMF and the W116F. The past multiple strong recent earthquakes, and the proximity, the SFS presents a ground-shaking hazard to the developed areas of Pahrump and Las Vegas.

ACKNOWLEDGEMENTS

TABLE OF CONTENTS

LIST OF FIGURES

CHAPTER 1

INTRODUCTION

The Stateline Fault system (SFS) is a major Quaternary age NW-striking right-lateral fault system in southern Nevada and southeastern California (Guest et al., 2007) (Fig. 1). The fault system as defined is controversial in both location and inclusiveness of local fault systems. Representing the eastern margin of the Eastern California Shear Zone (ECSZ), many aspects of the SFS remain controversial including its north and south extents, the timing of slip and its interaction with other faults. Initially defining the SFS, Liggett and Childs (1978) called attention to a set of NNW-striking strike-slip faults including the Ivanpah, Stateline, Mesquite-Pahrump, and Stewart Valley faults, all with evidence of dextral movement (Hewett, 1956; Malmberg, 1967; Fleck, 1971; Burchfiel et al., 1983). The Pahrump fault of Hoffard (1991) is now referred to as the Pahrump segment of the SFS (e.g., Guest et al., 2007). The Mesquite fault, Pahrump fault and Amargosa fault were grouped into the SFS and placed into the Eastern California Shear Zone domain (Guest et al., 2007) (Fig. 1). The southern Pahrump Valley and Mesquite section of the SFS was investigated by Scheirer (2010) and Hislop (2012). This fault system extends from Ivanpah Valley north to the Amargosa Valley. The approximate northern end of the SFS is variable in literature. It is suggested that the SFS extends in the sub-surface to the Yucca Mountain or Crater Flat areas through geophysical, structural, and geologic data (Donovan, 1991; Schweickert and Lahren, 1997; O'Leary, 2000; Guest et al.,

2007) (Fig. 1). The length of this fault zone as defined by Guest et al. (2007) is from the town of Primm, Nevada in the south to the town of Beatty, Nevada in the north, a distance of 200 km (Fig. 1). O'Leary (2000) shows the northern tip of the SFS extending east into the Yucca Mountain region, whereas Guest et al. (2007) show the SFS extending into the Crater Flat region. Both interpretations (O'Leary, 2000; Guest et al., 2007) result in a length of the SFS of ~200 km. The SFS is interpreted to extend through the west side of southern Pahrump Valley and the eastern side of Stewart Valley (Hoffard, 1991; Louie et al., 1998). Although few visible topographic features are apparent in the Pahrump and Stewart Valleys, the SFS location can be approximated through linear features such as cut washes and linear mesquite groves. Geophysical data also confirmed the existence of this fault at depth in Pahrump and Stewart valleys (Louie et al., 1998; Saldaña, 2009; Scheirer, 2012).

Estimates of the slip rate and lateral continuity of the SFS are variable (Schweickert, 1997; Bennett et al., 1999; Wernicke et al., 2004, Guest et al., 2007; Frankel, 2011). The geological estimates of 25-30 km of slip of the SFS since 12.75 - 13 Ma yields estimates of slip rate of 2.3 mm/yr (Schweickert, 1997; Guest et al., 2007). This observed motion over a large amount of time is in conflict with the modern observed slip rate for the SFS from regional geodetic data of 1.13 mm/yr (Bennett et al., 1999; Wernicke et al., 2004, Frankel, 2011) and the 0.9 mm/yr geodetically derived rate for the Amargosa segment of the SFS (Wernicke et al., 2004). This difference could be the result of (1) the fault

2

decreasing in strain rate, (2) differential strain buildup, or (3) the transfer of motion to a different fault such as in strain partitioning.

This fault is important due to its proximity to the population centers of Las Vegas and Pahrump, and the observations of young movement and surface ruptures (Hewett, 1956; Malmberg, 1967; Fleck, 1971; Liggett and Childs, 1978; Burchfiel et al., 1983; Hoffard, 1991; Louie et al., 1998; Guest et al., 2007; Saldaña, 2009). The inclusion of the Pahrump, Amargosa, and Mesquite faults in one long interconnected fault system by Guest et al. (2007) suggests the potential for a large magnitude earthquake and a significant hazard to the region (Fig. 2). An earthquake on the SFS would pose a major threat to the 2.5 million people of Pahrump, Las Vegas and the surrounding areas. This risk can be mitigated through a better understanding of the SFS tectonic history, ages of recent earthquakes occurred, frequency of earthquakes, lateral extent, and relation to other nearby active faults. The data can be applied to the future development of infrastructure and building codes with the seismic threat accounted for in construction design and allocation of resources for hazard mitigation of existing structures and infrastructure.

The possible change in the ratio of strike-slip and dip-slip components of motion along strike of the SFS where it crosses from the southern Pahrump basin into Stewart Valley is also of scientific interest. Detailed data about this change in slip will help understand the interactions of the SFS with the West Spring Mountains Fault (WSMF) (Workman et al., 2008) and the buried fault strand in Pahrump Valley in Carter et al. (2008), here referred to as W116 fault

(W116F). How these faults are interacting with the SFS will reveal a regional insight into how the tectonic stresses are being dispersed and strain partitioned. Hislop (2012) noted a similar along strike change in slip near the termination of the SFS in Mesquite Valley.

The primary focus of this thesis is on the characteristics of the SFS in Pahrump and Stewart valleys (Fig. 1). The SFS extends in a relatively straight line across the east margin of the Stewart Valley and overlain by intermittent linear and dense mesquite groves (Fig. 3). Washes in the east valley alluvial fan deviate north and south where they cross the fault (Fig. 3). The main SFS trace is located approximately in line with the mesquite grove several meters east of the valley playa and alluvial fan interface (Fig. 3). A secondary trace is visible in aerial photography and geologic maps east of the main trace in the southern trench site (Fig. 3).

CHAPTER 2

PURPOSE

The purpose of this research is to: (1) establish the exact surface location of the SFS in Stewart Valley; (2) to test whether the SFS is a continuous fault through Pahrump Valley into Stewart Valley; (3) to document, in a trench log, the location and the ages of recent ruptures; (4) to estimate the magnitude of prior earthquakes along the Stewart Valley section of the SFS; (5) to explain the change in slip sense through Pahrump and Stewart valleys, and (6) show if the SFS and/or any related faults aid in accommodating a change from regional strike-slip faults to the west and extensional faults to the east.

Research by dePolo et al. (2003) and Saldaña (2009) describe the lack of a fault scarp to be the result of the SFS fault motion mainly as subsurface and, for the most part, strike slip in the region. This conclusion leaves a possibility that the fault may not be continuous or intercept the surface as it passes through Stewart Valley. A close approximation of the SFS in the subsurface at Stewart Valley has been discovered using geophysical surveys (Saldaña, 2009) (Figs. 4 and 5). It is possible to gather more data about the fault and its past from other investigative geologic methods such as paleoseismic trenching. The total length of the SFS is still being established and needs to be verified (Hewett, 1956; Malmberg, 1967; Fleck, 1971; Liggett and Childs, 1978; Burchfiel et al., 1983; Guest et al., 2007).

In order to document the hazard of the SFS it is important to understand the total surface rupture length (SRL) of the fault. The SRL of a fault correlates to the

observed earthquake magnitude on a fault (Hanks and Boore, 1984; Wells and Coppersmith, 1994). Using the relationship between fault length and earthquake magnitude, the SRL can be used to establish the largest size earthquake that a fault is likely to produce (Wells and Coppersmith, 1994). This information can then be applied to improve future building codes and disaster plans for local communities. Saldaña (2009) established an understanding of the SFS using seismic interpretations. The goals of Saldaña (2009) were to utilize seismic reflection to locate the SFS in Stewart Valley and also produce a pseudo-3D reflection survey showing the sub-surface geometry of the fault and estimate the slip rate of the fault system. The seismic study performed by Saldaña (2009) also displayed an interpreted debris flow on both sides of the SFS that shows offset across the fault. This offset along with an estimated age of the sediments as mid to late Pleistocene in age gives a Quaternary slip rate of 6.5 mm/yr +0.9 -0.8 mm. The thesis also shows the SFS exhibits a flower structure geometry at depth.

This project will also investigate the SFS in a region with an apparent change in fault motion type as shown by the change in the SFS scarp height where it traverses from Pahrump Valley into Stewart Valley. In Stewart Valley, a visible fault scarp is lacking along the SFS (dePolo et al., 2003; Saldaña, 2009). In Pahrump Valley, previous mapping in the southern valley by Workman et al. (2008), and geophysical surveys (Louie et al., 1998), show multiple fault scarps on the SFS with large vertical offsets (10 m to 15 m; Louie et al., 1998; Workman et al., 2008). This vertical offset is in conflict with the characteristics exhibited by the SFS in Stewart Valley where the fault scarps are not readily detectable

6

without survey equipment, which suggests strike slip motion. This difference

establishes a need to document what is happening to the vertical component of

this scarp forming fault motion.

CHAPTER 3

BACKGROUND

3.1 Regional Tectonic Domains

The SFS lays in the overlap area of the Central Basin and Range province (CBR), Eastern California Shear Zone (ECSZ) and Walker Lane Belt (Fig. 6). The CBR is defined by Wernicke (1992) as lying between the Sierra Nevada and Colorado Plateau between 37° N and 35° N latitudes (Fig. 6). The western edge of the CBR contains right-lateral strike-slip faults of the ECSZ and Walker Lane Belt, but to the east contains normal faults, some of which are Quaternary in age (Wernicke, 1992; USGS, 2005) (Figs. 2 and 6). The SFS lies near the interface between the strike-slip and normal faults. The main differences between the Walker Lane Belt and the ECSZ are just the defined locations and the greater number of left-lateral strike-slip faults in the Walker Lane Belt. The ECSZ is defined as series of mid-Cenozoic and younger dextral-slip and normal faults with steep dip, right slip and en echelon segments related to the Basin and Range extension (Dokka and Travis, 1990; Wenousky, 2005). The Walker Lane Belt is also dominated by NNW-striking dextral faults. The Walker Lane Belt is divided into nine domains by east-northeast striking left-lateral faults extending from the northern Sierra Nevada south to the Garlock fault (Stewart, 1980; Stewart, 1988; Oldow et al., 1994; dePolo, 1998; Wesnousky, 2005; Wesnousky et al., 2012). Both domains overlap in the CBR.

8

The ECSZ and Walker Lane Belt accommodate right-lateral slip from the transform margin between the Pacific and North American plates. This motion is associated with Miocene to Holocene strike-slip, normal and reverse faults east of the San Andreas Fault system (DeMets and Dixon, 1999; Bennett et al., 1999; McClusky et al., 2001; Surpless, 2008). These zones relieve as much as 20-25% (9.5-13 mm/yr) of total relative motion (49 mm/yr) of the North American and Pacific plate boundary (Sieh and Jahns, 1984; Hearn and Humphreys, 1998; DeMets et al., 1987; DeMets and Dixon, 1999; Gan et al., 2000; McClusky et al., 2001).

The regions of the CBR, ECSZ, and Walker Lane Belt have active faults with documented recent earthquakes. Some of the major active faults of the CBR are shown in Figure 2 (Anderson, 1999; Saldaña et al., 2006; dePolo et al., 2006) (Figs. 2 and 6). The ECSZ and Walker Lane Belt include active faults such as the Death Valley-Furnace Creek, Fish Lake Valley, Hunter Mountain-Panamint Valley, and Owens Valley fault zones (Frankel et al., 2008). The 1999 Hector Mine (M7.1), 1992 Landers (M7.3), 1932 Cedar Mountain (M7.2), and 1872 Owens Valley (M~7.6) earthquakes occurred on faults within this region. These active faults and recent large magnitude earthquakes establish a hazard for the local populations in the CBR

.

3.2 Regional Slip Rates

The slip rates along the SFS in Stewart Valley and Pahrump Valley during the mid-Miocene (2.3 mm/yr) compare well to the regional slip rates during the mid-

Miocene. The SFS has an average slip rate since mid-Miocene of 2.3 +/- 0.35 mm/yr (Guest et al., 2007). This rate is from displaced deposits at Black Butte to the source material at the Devil Peak intrusion. This paired source and deposit gives a good representation of the offset of the SFS.   Slip rates along similar faults in nearby systems are: Death Valley (1-3 mm/yr, Klinger and Peity, 2000), Panamint Valley (2.4 mm/yr, Zhang et al., 1990), Hunter Mountain (2.0-3.2 mm/yr, Oskin et al., 2007), and Owens Valley fault systems (1.4-1.6 mm/yr, Beanland and Clark, 1994).

The average mid-Pleistocene to Pliocene slip rates for the SFS are twice that of modern geodetic rates (Guest et al., 2007). The difference between the rates is not typical of other ECSZ faults (Guest et al., 2007).

CHAPTER 4

METHODS

The following methods were applied in order to: (1) establish the location of the SFS, (2) test the lateral continuity, (3) establish ages of recent events, (4) establish changes of slip sense along strike, and (5) establish the size of past and possible earthquakes along the SFS.

4.1 Paleoseismic Trench

To establish the surface location and timing of any past earthquake events, a cross-fault trench survey was performed across the SFS. The information that can be gained using this approach includes fault locations, fault complexity, specific dates of earthquakes on the fault, and the fault geometry. To better locate and define the SFS history of activity, three trenches were excavated. The sites were determined using a combination of surface survey investigation, aerial photography and observations across the interpreted fault trace. These trenches were located in Nye County, approximately 10 km west of the town of Pahrump and 2 km east of the state line between Nevada and California (Fig. 3). The trenches were located in playa and alluvial sediments at the eastern margin of the Stewart Valley playa. These sites are where previous surficial mapping by Guest et al. (2007) and dePolo et al. (2003), reflection geophysical work by Saldaña (2009) and other geophysical studies by the Applied Geophysics Center at UNLV indicated the location of the SFS at depth. On the surface, minimal

11

topographical rise is associated with the fault trace in Stewart Valley. The surficial mapping performed by dePolo et al. (2003) and later confirmed by Saldaña (2009) confined the fault trace to a narrow (30 meter) corridor.

The approximate location of the fault trace was also detected using a Topcon robotic total station to detect and document elevation changes (Figs. 7, 8, and 9). Linear discoloration of sediments in aerial photography and a conspicuous lineation of a playa margin mesquite grove confirmed the location of the fault traces. These data together establish the most likely location of the fault where it intersects with the surface (Fig. 9).

The trench study of the SFS involved excavating trenches at two locations crossing the fault in Stewart Valley. The trenches were excavated in December of 2009 and filled in June 2009. The trench locations were chosen to cross the fault perpendicular to the strike so that the originally horizontal and continuous sediment horizons in the trench would reveal information about the fault kinematics and a history of fault activity where the fault traces offset them as defined in Birkeland (1999). Typically, a paleoseismic trench study of a strike-slip fault would also include a pair of strike-parallel trenches on both sides of the fault to demonstrate offset of originally linear features that cross the fault. In this study, used pseudo-3d seismic data previously collected by Saldaña (2009) (Fig. 4) as strike parallel trench data would have been redundant.

The trench locations were adjusted short distances north and south using the input of BLM officials on areas of lowest potential environmental and archaeological impact. This resulted in one trench site location as far north as

geologically acceptable in Stewart Valley to establish continuity of the fault

through the valley (Fig. 3). The other site was placed as close as feasibly

possible to the site examined by Saldaña (2009) (Figs. 3 and 4). The site was

selected to complement the Saldaña (2009) survey and data from a well log

(discussed below). This allows for depiction of the SFS from the shallow

subsurface to the surface intercept (Figs. 3, 4, and 5). Due to an unavoidable

along strike offset of the seismic reflection profile line with the locations of the

southern trench sites, the fault strands may have slightly different locations in the

different data sets (Figs. 3, 4, and 5). A test well was drilled by Eagle Drilling for

the University of Nevada, Las Vegas Applied Geophysics Center near the

Saldaña (2009) seismic survey site. The intention was to better relate trench and

seismic reflection. A star marks the test well location in Figure 4. Appendix 3

presents the data gathered from the logged well core and chip sediment types.

4.2 Trench Log Construction

The excavation of the trenches was designed so that the south facing wall

was cut at a relatively shallow slope for safety while the north trench wall was cut

vertically to best preserve the soil and sediment stratigraphy, and fault traces for

data observations. Trenches can display fault traces as discontinuities or offsets

in horizontal sediments in the trench face. The location of the fault splays, vertical

offset and the relative ages of events can be determined from the relation of cut

and uncut sediment and their ages.

The trenches were documented using a photomosaic. After establishing the

units and locating the fault surfaces, the trench walls were digitally photographed

in a series of multiple close-in photographs that were then merged into a digital

mosaic covering the entire trench wall. The photographs were made with a

vertical pole with a bubble level and digital camera attached to a slide that can

move vertically. A series of photos were taken of the trench face at overlapping

intervals. Due to the limited width of the trench, the photos were taken at a

distance of roughly 0.5 meters away from the trench face. The mosaic

construction process and documentation was aided by (1) a string grid of 0.5 m

vertical intervals and 1 m horizontal internals and (2) roofing nails with colored

tags that were placed into the trench face along sedimentary horizons and fault

surfaces. Although parallax from uneven surfaces caused a doubling of features

in the mosaic, the resulting photographs show a complete mosaic of the

sediment horizons highlighted by colored nails inside of a string grid. Using

photographic editing software (Adobe Photoshop), the photos were then

processed to reconstruct the string grid and trench face surface between each

image. Using the individual photos and mosaic images, an accurate trench log

was created that depicts the trench features (Fig. 15, Plate 1).

4.3 Soil/Sediment Dating

Dating of the fault activity is dependent on the sediments that have been

disturbed and not disturbed. It is possible to use logged fault strands that do not

cut completely through to the surface to constrain the age of the fault strand in

relation to the age of the host sediments. Using the ages of cut and uncut beds that are closest to the fault strand tip, the timing of the motion on the strand is then bracketed to have occurred between the ages of the two beds. The overlying uncut sediment constrains the youngest age of motion whereas the fault-cut bed date constrains the oldest age of the fault motion (Fig. 10).

The sediments from this study were dated using radiocarbon methods. The $^{14}C/^{14}N$ system is used to show an age of soils or sediments that contain enough preserved organic carbon. The ^{14}C isotope forms from the interaction of cosmic rays with ^{14}N by neutron capture. The passage of time results in the unstable ^{14}C reverting back to ^{14}N by beta decay. This process allows for a mostly constant ratio of ^{14}C and ^{14}N existing in the earth's atmosphere. Although small deviations in the ratio occur through time, this deviation is compensated for in the final date calculations mostly through comparisons with dendrochronology. Living organisms aspirate this ratio of ^{14}C /^{14}N while alive, constantly keeping aligned with the atmospheric ratio. When an organism dies, it no longer exchanges this isotope and the isotope present inside the organism decays at a predictable rate. This is the start of the "^{14}C clock". As the decay occurs, the resulting isotope is not replenished in an equal proportion to the ^{14}N and results in a different ratio dependent on how long the organism has been dead. This relationship is important because if organic carbon is found in a sedimentary layer it can be related to a time of deposition of the sediment.

Radiocarbon samples were collected from the trenches by using a stainless steel trowel and the sediments were placed in an aluminum foil wrapper. The

initial trench material exposed to the air was discarded and approximately 1 liter

of sediment dug from the trench face was collected. The radiocarbon samples

were collected from horizons that lie above and below fault tips. The selected

locations were far enough away from the faults to avoid possible contamination

of the sample material with modern carbon via the fault surface acting as a fluid

conduit. PaleoResearch Institute was contracted to examine the collected

samples for identification of carbon type, identification of fossils and pollen, and

radiocarbon analysis. Red stars in Plate 1 designate the radiocarbon sample

sites.

4.4 Well Log Lithology Database

In an effort to document the subsurface character of the SFS as it passes

from southern Pahrump Valley into Stewart Valley, a well log database of 1,283

lithologic records from local water wells ranging in depth of 20 feet to as much as

2000 ft was constructed. Water well logs filed with the Nevada Division of Water

Resources were used. This well log database catalogs the sediment grain size in

relation to the depth at which it was collected from the well. It is possible to

visualize the basin sediments in Pahrump Valley with this database and to

visualize displacement caused by tectonic motion that disrupts units that were

uniformly deposited from normal basin-fill sedimentation. Well logs were entered

into Rockware Rockworks software and depicted in a 3D model of the basin

sediments. Due to the variable quality and multitude of sediment descriptions of

the water well logs, the units described in the 3D model were redefined into nine

units based on overall grain size and unit description. Wells were spatially located using street addresses of the drill sites, UTM coordinates if included and at worst, the location of the public land survey system location listed on the well log. Wells were further filtered to best display the deepest sediments and very shallow wells were only included if there were no other nearby deep wells. Erroneous and illegible well logs were not used. 1,283 wells were cataloged covering the entire city of Pahrump and northern Pahrump Valley (Fig. 12).

4.5 Fault Scarp Profiles

When an earthquake occurs and displacement causes a normal or strike-slip rupture at the surface where loose materials are present, the resulting discontinuity across the fault surface forms a fault scarp. These surface features remain until erosion levels the soil or sediment back to the original surface profile. Profiles of fault scarps can be used in determining the history of fault motion because erosion takes time. Scarp profiles reflect the number of scarp forming events. Erosion acts on parts of the scarp that are exposed longer than the portion of the scarp that is more recently formed (Fig. 13). When newly formed, fault scarps are relatively steeply inclined and have angular non-sinuous surfaces. As erosion acts on this surface, it becomes more sinuous in profile and less steep. Consecutive earthquakes then steepen the lower part of the scarp again. This repeated cycle causes "bevels" in the profile that can be interpreted as separate strong earthquake events. Typically, scarp shape can also be used to determine the age of each event through diffusion calculations. In the case of

the SFS however, which is documented to have a large component of strike-slip, this calculation would be inappropriate due to the possibility of uneven scarp topography transported along-strike causing the amount of vertical change to be inconsistent with the amount of erosion and time passed since the last earthquake (Bucknam and Anderson, 1979). The fault scarp profiles are useful to estimate the number of scarp forming earthquakes on the SFS recent enough in time not to have eroded.

For this study, scarp profiles were taken orthogonal to the fault strike. The profiles for this study were taken adjacent to the trench site locations in order to show the change in topography where the fault disturbed the surface (Fig. 9). Where obstructed by vegetation, the profiles were taken again with an along strike offset and profile overlap (Figs. 8, and 9). The intention of this overlap was that the two shorter profiles where interrupted by vegetation could be overlapped onto each other in a graph and still represent a continuous sense of the gradient of the alluvial slope. Profiles were collected to the south of the entrance to Stewart Valley in northern Pahrump Valley (Fig. 9). As previously stated, the surveyed scarp profiles could not be used to produce a diffusion model due to the lack of sufficient elevation change and complications in applying this approach to strike-slip faults. However, the fault scarp profiles give insight into the location of the fault splays near the trench and the number of scarp forming earthquakes along the SFS.

4.6 Surface Rupture Length

The along-strike length of a surface rupture is used to estimate a maximum possible magnitude that the SFS will generate if an earthquake occurs. If the SFS is a continuous fault system underground, then a linear relationship of the surface rupture length to magnitude of an earthquake can be applied to estimate the largest possible earthquake magnitude of the SFS. Wells and Coppersmith (1994) demonstrated that magnitudes of instrumentally observed earthquakes are related logarithmically to the associated fault surface rupture length. This relationship is used to generate a formula relating a surface rupture length of a non-instrumentally recorded earthquake to an earthquake moment magnitude. The formula for linear regression of the surface rupture length to the magnitude is (*M=5.08+1.16*log (SRL))* where "M" is Magnitude and "SRL" is Surface Rupture Length. This equation can show a maximum possible earthquake magnitude for a fault that has no previous instrumentally recorded magnitudes (Hanks and Boore, 1984; Wells and Coppersmith, 1994) (Fig. 14). It is important to note that the fault may not rupture entirely along its length in an earthquake and that the estimated magnitude reflects a "worst case scenario" earthquake.

CHAPTER 5

DATA

To better define the characteristics of the SFS in Stewart Valley and Pahrump

Valley the following data were gathered. (1) Sediment descriptions of each

horizon exposed in the trenches including relative ages and textures were

constructed. (2) Topographic profiles of the SFS scarp on the alluvial fan

surfaces in both Stewart Valley and in northern Pahrump Valley near Stewart

Valley were collected. (3) A structural examination was performed that constrains

the: (a) number and geometries of; (b) locations of; and (c) the relative and

approximate ages of fault surfaces with an emphasis to determine information

about the most recent fault activity, earthquake magnitude and recurrence

interval. (4) Determine the ^{14}C ages of units that bracket the fault traces. (5) A

well log lithology database was constructed to aid in establishing the extent of

splays of the SFS in Stewart Valley and Pahrump Valley.

5.1 Paleoseismic Trench Study

Three trenches totaled 252 m long and averaging 1.5 m deep and 1 m wide at

the bottom The north trench comprised an 88 m long trench in northern Stewart

Valley at the location 36°15'33.43"N and 116°10'24.78"W (Fig. 3). The two other

trenches were excavated along a straight line at 36° 13' 22.811"N, 115° 55'

48.001"W and 36° 13' 28.467"N, 116° 9" 11.037" for the southeast trench (45 m

in length) and 36° 13' 27.000"N, 116° 09' 15.390"W and 36° 13' 25.930"N, 116°

9' 18.520W for the southwest trench (119 m in length) (Fig. 3). Initially the southern trenches were planned to be a single continuous trench. However, the lack of features in the center segment of the trench and the time and cost to excavate a complete single trench resulted in a compromise of cutting two shorter trench segments instead.

Both the southwest trench segment and the north trench contain the main trace of the SFS (Figs. 3 and 5, Plate 1). The southeast trench and the southwest trench contain splays to the main fault array (Fig. 5, Plate 1). In the north trench, the main fault trace was observed but either the other fault splays are not preserved in the soil and sediment enough to discern or they are not present in the north trench (Plate 1).

Normally any observed fault strand would be verified by examining soils and sediments in both sides of the trench. In this trench survey, the excavation design made it difficult to document observations in the opposite wall of the trench due to the south face of the trench being sloped to increase safety from the risk of a trench wall collapse. In a few cases, the sloped side of the trench was excavated with a shovel to locate a fault on the opposite side of the trench.

5.1a Sedimentary Units and Dates

The trench walls show five distinct units in sediment or soils defined by changes in color, cohesion, overall grain size, fracture habit, texture, grain sorting, and overall resistance to erosion. The units are dominantly very fine-grained playa and distal alluvial fan sediments ranging in size from silt and clay

to coarse sand. These units were divided based on usefulness to documenting fault offset rather than soil development or depositional environment. The unit designations do not preclude that they could be parts of one or more soil packages. Two features developed within these units also were identified. The trench unit numbering is defined using Miall's (1990) nomenclature of the smallest number at the top of the trench.

Three of the defined units are common to the north and south trench sites: units 1, 2, and 3. Liquefaction features, krotovina, and brecciation were documented in all of the trenches, but these features mainly occurred in unit 2, near the contact of units 2 and 3, and in unit 3 in the southern trenches. Fault strands traverse and offset all of the trench units except unit 1. Observed fault strands are accompanied by localized brecciation in units 3 and 4.

UNIT 1

The uppermost trench unit, unit 1, is composed of grayish orange (10YR 7/4) to pale yellow brown (10YR 6/2) silty and sandy clay with weakly to unconsolidated particles. The unit is an average of 10 cm thick and ranges from 1-30 cm thick. There is no visible bedding or foliation. The lower contact is gradational and defined by cohesion from the ability of the soil to hold a nail. Unit 1 cannot hold a nail perpendicular to the trench wall. Fine roots and organic particles are present in this unit, especially near the mesquite grove segments of the north and both south trenches. This unit contains the modern soil. A carbon

sample date of 1956 AD underlies the unit, near the unit 1 and 2 contact, but contamination through fractures may be an issue.

UNIT 2

The second lowest unit from the trench surface is unit 2. This unit is defined by moderate yellow brown (10YR 5/4) to yellowish brown (10YR 4/2) silty to sandy clay of medium to very fine grain size. The unit has medium to strong induration that shows columnar fracture and massive bedding. This unit contains cracks and prolific fine roots. The cracks show a preference to form horizontally near the top of the unit and have multiple orientations lower in the unit. White, 1.5 to 0.5 mm size nodules of carbonate are randomly dispersed throughout this unit. The upper and lower contacts are gradational and planar overall but locally wavy. The unit averages 60 cm thick but varies from 10 to 150 cm.

Radiometric carbon dates of particulate soil organics taken near the contact between units 1 and 2 (sampled just below the unit contact inside of unit 2) provide three possible ^{14}C ages with the youngest age of 1956 AD (Fig. 16, Plate 1, Appendix 1). This date may be overly young due to contamination. A date of 1956 AD would intuitively be at or very near the trench surface. In addition, the area had American settlers at that time but no earthquakes were reported. Particulate organics taken from soil in the middle of unit 2 yields an age range of 680-560 cal yr B.P. (Fig. 16, Plate 1, Appendix 1). The radiometric carbon date from charcoal in the middle of unit 2 yields an age range of 1060-930 cal yr B.P. (Fig. 16, Plate 1, Appendix 1).

UNIT 3

The third lowest unit from the trench surface is unit 3. This unit is a mottled pale yellow brown (10YR 6/2) and grayish orange (10YR 7/4), when wet, fine-grained sandy clay. In the west portion of the northern trench, the unit is composed of a dusky yellow (5Y 6/4) very fine-grained sandy clay. The entire unit is moderately to very well indurated exhibiting variably massive to faint 20° west-dipping thin crossbeds. The upper portion of the unit shows cracks, vesicles and columnar appearance. The cracks form a more "blocky" orthogonal pattern than in unit 2. The color of the sediment also has correlation to the induration; where the unit is lighter in color, its cohesiveness increases. The upper unit contact is gradational and locally wavy but overall planar. The unit is an average of 75 cm thick varying from 30 to 150 cm in thickness.

The radiocarbon dates from sediments in unit 3 range from 3340-3210 cal yr B.P. to 8640-8550 cal yr B.P. A sample of humates (soil organic compounds) taken inside of unit 3 just below the boundary between units 2 and 3 yielded an age of 3340-3210 cal yr B.P. (Fig. 16, Plate 1, Appendix 1). Unidentifiable charcoal and particulate soil organics located in unit 3 yielded a radiocarbon age of 8640-8550 cal yr B.P. (Fig. 16; Plate 1; Appendix 1).These two dates are inconsistent. The sample yielding the 8640-8550 cal yr B.P. date may not represent the hosting unit. This date may be the result of the transport of older carbon into the unit and resulting in an older sample date than the age of

deposition. Alternately, uneven deposition rates along the alluvial surface may result in different ages at similar stratigraphic depths in different trenches.

UNIT 4

The fourth lowest unit from the trench surface is unit 4. This unit is very pale orange (10YR 8/2) to greenish grey (5GY 8/1) carbonate-cemented clay containing fine- to coarse-sized concretions of clay and carbonate grains, that are angular to sub-angular in shape. This unit shows massive bedding, sharp contacts, medium to strong induration with brecciation and discontinuity near fault traces. This unit is only visible in the northern trench due to the shallow depth of the southern trenches. The unit averages 0.5 m thick but varies from 0.5 m to 1.7 m thick. No samples of this unit were dated.

UNIT 5

The fifth lowest unit is unit 5. It is very pale orange (10YR 8/2) to variably pinkish grey (5YR 8/1) to grayish orange pink (5GY 7/2) and contains assorted carbonate cobbles that are rounded to sub-rounded in a carbonate-cemented matrix. Cobbles comprise 30-40% of the carbonate matrix. Overall, the entire unit is greater than 70 cm thick. Unit 5 is moderately indurated but less than the above layer. No bedding is visible. Upper contact is sharp to gradational and overall planar. The lower contact is not exposed. Layer shows severe brecciation near fault surfaces. No samples of this unit were dated. This unit is only exposed in the north trench.

In-unit hosted features

Two types of non-laterally continuous features are documented in the trench. (1) The first feature is krotovina, which are the semi-circular remnants of animal burrows that have filled in with younger sediments from upper strata. These features leave rounded circular deposits that exhibit thin-bedded layers that contrast with the host sediments (Fig. 11, Plate 1). (2) Also present are liquefaction features. Liquefaction features form from lower sediments, predominantly sand, that migrated vertically up stratigraphically and were emplaced as distinct massively bedded bulbous forms that terminate with sharp angular contacts abruptly against more cohesive overlying layers (Fig.11, Plate 1). Liquefaction feature morphology is distinct in contrast to the small; more round and horizontally bedded krotovina.

Krotovina

This feature is defined as small sandy inclusions ranging from 2-10 cm in diameter averaging 7 cm diameter, which occur in units 2 and 3. The features are oval to circular shaped pockets of grayish orange (10YR 7/4), friable sand. Size of particles ranges from fine to medium grained. The pockets show very little cohesion and sharp contacts with the host material. Weak horizontal bedding is apparent. No roots were present in this feature.

Liquefaction Features

This unit is similar to krotovina in that it occurs within another unit but the feature morphology is different and bedding is indistinct and massive. These features form multiple pockets of grayish orange (10YR 7/4), friable sand. The size of particles ranges from fine to medium grained. These features show very little cohesion and sharp contacts with host material. The typical morphology is generally oval packets that pinch out laterally in sharply pointed terminations parallel to bedding. These features are present in units 1, 2 and 3. They range in width from 7 cm - 200 cm, and average 40 cm. Vertical thickness ranges from 10 cm - 25 cm, averaging 20 cm. No roots were present in these features.

The observed type of liquefaction features in the trenches is loosely consistent with the "ground oscillation mechanism" defined by the National Research Council (1985). The decoupling of overlying sediment horizons causing fissures that then fill with the underlying sediment.

5.1b Faults in Trenches

Fault locations

This study documents multiple fault strands that range in profile length within the trenches from 1.5 to ~6.5 m (Plate 1). The faults display no readily identifiable fault scarps on the surface near the trenches. Locations of fault surfaces were taken in reference to the same grid point at the west trench entrance. Observed vertical displacement (throw) across fault strands ranges from detectable (fault was observed by presence of fault gouge) to 20 cm of total vertical offset of a unit contact. Cumulatively the southwestern trench segment shows 0.7 m of vertical

fault displacement. This displacement is represented as a down-to-the-west displacement across all of the sediment horizons, except in the youngest unit contact, over a 25 m horizontal distance. The overall displacement across the northern trench is a 1.5 m increase of elevation over a 30 m horizontal distance (Plate 1). The contact between units 2 and 3 is the best marker horizon for preserving offset from fault motion. Just below and at this unit contact is the most common location for the liquefaction features to occur (Plate 1).

The strike direction of the main fault array is generally north northwest as observed in both trench faces with dips that vary from 30°W to 45°E. Both the north and the south trenches share a common fault array cutting the unit 2 and unit 3 contact that strikes 350°. In both trenches this fault array occurs where the trench passes through the mesquite grove.

5.1c Fault Surfaces in Trench Log

Southwestern Trench Fault Data

Fault BB

A fault, evident from fault gouge that tapers upward from 5 to 1 cm wide, is present ~28.5 m east from the west end of the trench (36° 13' 26.339" N, 116° 9' 17.629" W). The fault is visible in both sides of the trench and forms a fault plane oriented at 350°, 88° E. The fault cuts the contact between units 2 and 3 and shows vertical separation of 0.25 m west side down (Plate 1).

Fault Array CC

Thirty nine meters east of the west end of the trench (36° 13' 26.430" N, 116° 09' 17.100" W), an array for faults is exposed. The array consists of four visible faults (C1, C2, C3, C4) and four faults inferred(C5, C6, C7, C8) from unit offset but with no directly visible surfaces, show ~45° W dip on the west faults and ~35° E dip on the east surfaces. The fault surfaces displace the contact between units 2 and 3 with both reverse and normal vertical offsets of an average of 0.25 m per surface assembling an extensional flower structure (tulip structure). Total net throw across the tuplip structure is a 0.15 m drop to the west of this contact. The sediments cut by the array were sampled for ^{14}C (Appendix 1, samples SWT011 and SET012). The lower cut horizon is bracketed to be 1060-1020 or 1010-930 cal yr B.P. (Plate 1, Appendix 1). The higher uncut soil yields modern dates of 1956-1997AD, which most likely are from contaminated samples (Plate 1, Appendix 1). All of the documented strands except fault strand C1 terminate at this dated horizon. C1 terminates at unit 1. This may indicate that strand C1 is the result of a younger event or that a younger event also occurred along it.

Fault DD

Eighty four meters east from the west trench end, a fault was identified from an 8 cm down-to–the-west offset of the units 2 and 3 contact and the proximal location of a steeply dipping sand feature along the fault trace of a liquefaction inclusion. Fault dip and direction are not readily apparent but the fault is observed to be near vertical. Offset of the fault extends through unit 3 into unit 2.

Southeastern Trench Fault Data
Fault EE

The southeastern trench exposed two fault surfaces (E1, E2), which are evident from white fault gouge and linear fracture sets that were present in both sides of the trench at 19 m east from the west end (36° 13' 26.205" N, 116° 9' 16.950" W). These fault surfaces show two planes of orientation at 340°, 70 ° E. These fault surfaces truncate at the contact between units 3 and 4. The age of these faults is estimated from the ^{14}C of those units as older than 680-560 cal yr B.P. and 3340-3210 cal yr B.P.

Brecciation FF

The southeastern trench has a 3 m wide region, located 30 m east from the west end of the trench, of units 2 and 3 that is brecciated. This zone exhibits large inclusions of liquefaction features in both layers and unit contact disruption. Disruption of the unit contacts has vertical variability of 0.25 m as seen in the trench face (Plate 1). Brecciation occurs in units 2, 3 and 4. No single fault surface is visible but the brecciation is likely the result of fault motion along a zone.

North Trench Fault Data
Fault GG

A fault surface was present in the north trench at 36° 15' 32.18" N, 116° 10' 28.13" W and is ~53 m east from the west end of the trench. All of the trench

sediment units except units 1 and 2 are offset. The width of the fault zone decreases upward. Units 4 and 5 show brecciation and contact disruption. Offset is 0.5 m down-to-the-west with a dip of 40°W. The strike is estimated to be 340° Units 2 and 3 display less offset but across a single fault surface.

Fault HH

A fault, evident from a 9 cm down-to-the-west drop of units 5 into unit 3, is present at 34 m east from the west end of the trench (36°15'32.77"N, 116°10'28.27"W). The fault age is constrained using radiocarbon AMS dating of the uncut sediments to older than 3340-3210 cal yr B.P. (Plate 1, Appendix 1). The fault shows vertical displacement of 0.25 m of all cut units.

Fault II

An abrupt offset of units 4 and 5 is apparent at 38 m from the west trench entrance but an obvious fault trace is lacking. Unit 5 is brecciated near this offset. The dip is estimated to be 60°W (Plate 1). Fault offset is 0.25 m down-to-the-east of the units 3 and 4 contact and is ~0.4 m down-to-the-east at the unit 4 and unit 5 contact.

Fault array JJ

At 41 to 48 m from the west end is an array of faults (J1, J2, J3, J4) offsetting units 3, 4, and 5 at their contacts. Overall, fault array JJ offsets the units 4 and 5

contact more than the units 3 and 4 contact with a net down-to-the-west

displacement of about 0.5 m. The estimated strike of the fault is 330° (Plate 1).

Fault J1

This fault is 48 m from the west end of this trench and is a single strand

dipping 35° W that cuts the units 4 and 5 contact. The strand offsets the unit 4 / 5

contact 0.4 m down-to-the-west. Fault J1 is shorter than the other JJ faults.

Visibly the fault surface extends upward almost to the units 4 and 3 contact but

does not cut it. The strand is exposed for a length of 1.8 m along the trench face

(Plate 1).

Fault J2

This fault is 48.5 m west of the trench end and is near fault J1 but 0.2 m east.

This fault has three splays that separate in unit 4 and the fault surfaces are

visible as fractures with offset that can be traced through units 3, 4 and 5. The

contacts are offset in a down-to-the-west sense by about 0.5 m for all of the

splays with the unit contacts except the furthest east splay which displacement

was 0.1 m to the west. The fault plane has a variable dip that gradually becomes

more horizontal from unit 5 and the trench floor interface (35°) to the unit 4 and

unit 3 contact (10°) (Plate 1).

Fault J3

This fault surface does not have a visible surface but is identified from abrupt offset of the contact between units 4 and 5 in conjunction with localized brecciation within the hosting units. Offset is 0.2 m down-to-the-west. The fault trace as inferred from the unit offset dips generally 45° W (Plate 1).

Fault J4

This fault surface cuts part of unit 3, unit 4, and unit 5. Due to brecciation, the trace is not directly observable in unit 5. Offset of the contact between units 4 and 5 is 0.5 m but the offset at the unit 3 / 4 contact is only 5 cm. The fault plane has a variable dip that gradually becomes more horizontal near unit 5 and the trench floor interface (33°) to the unit 4 and unit 3 contact (7°) (Plate 1).

Brecciation KK

At 26 m east from the west end of the trench (36°15'32.59"N 116°10'28.38"W), brecciation was observed in unit 4 over a 0.5 m horizontal length. This could be the result of a fault or liquefaction but is indeterminate as to which due to the lack of injection features or offset (Plate 1).

Brecciation LL

At 23 m east from the west end of the trench (36°15'32.55"N 116°10'28.59"W), brecciation was observed in unit 4 over a 0.5 m horizontal length. No offset of the overlying layer contacts and no injection features were present (Plate 1).

5.2 Scarp Profiles

In the Amargosa segment and in southern Pahrump Valley on the Pahrump Valley segment, the SFS exhibits visible fault scarps of 1 to 25 m (Hoffard, 1991; Workman et al., 2008). In Stewart Valley, scarp heights are less than 1.5 to 5 m. The SFS was approximately located using a total station (Figs. 7, 8, and 9). The west sloping alluvial fan surface on the east side of Stewart Valley displays a variable 1.5 to 3° change in down slope gradient before and after traversing a fault splay in a transect measurement (Figs. 7, 8, and 9). The SFS scarp disturbs downhill erosion of the alluvial fan which is evident in surveyed transect profiles as bevels in segments of an otherwise regular slope (Figs. 8 and 9)

The north trench profile survey and north point fault scarp profile show that the alluvial fan has an average of 0.4° slope at the north trench site and that there is 0.5 m vertical elevation offset from the normal slope near the mesquite grove (Figs. 7 and 8). The total profile change in elevation was 1.9 m and the profile shows three bevels across the surveyed 175 m (Fig. 8).

The South Road total station transect (profile) shows that the alluvial fan has an average of 0.7 degrees with 0.7 m of vertical offset observed from the scarp. The total elevation offset was 4 m and the profile shows three possible bevels across 315 m (Fig. 8).

The survey profile of the south Stewart Valley scarp near the trench site has an average of 0.5° slope across the alluvial surface and four separate 0.5 to 0.3 m vertical offsets of the slope (Fig. 9). The total change in elevation across the

34

profile was 7.1 m. Due to obstructions the south trench profile was taken in two overlapping but north-south shifted transects and combined into one transect. The profile shows four changes in gradient across the combined two profiles of 490 m (Figs. 7 and 9). The south Stewart Valley scarp profile has an average slope of 3° and three distinct bevels (Fig. 9). The total change in altitude crossing the scarp is 16.6 m over a distance of 312 m (Fig. 9).

For the measured fault scarps, a diffusion rate was not calculated because the fault motion type, observed as dominantly strike slip, invalidates the age diffusion modeling processes (Hanks and Boore, 1984). The Stewart Valley fault scarp has vertical offset of 1.7 m in the north of Stewart Valley to 15 m measured in the south of Stewart Valley (Fig. 9). The fault scarp slope observed in Stewart Valley is 1.5 m over 100 m of horizontal distance, while the slope of the Pahrump Valley scarps is 15 m over 100 m of horizontal distance.

In Pahrump Valley on the west alluvial surface of the Spring Mountains, the WSMF main trace scarp was profiled. The scarp measured in profile at 7.5 m and 9 m high and extended a horizontal distance of ~100 m. The scarp slopes are 7.5° of the WSMF scarp #1 and 11° of the WSMF scarp #2. Both profiles show two offsets, ie., a bevel and the most recent scarp. A common more recent 2.5 m offset in the profile. Diffusion modeling was not performed on the WSMF scarps due to the presence of multiple bevels, which invalidates the modeling process (Hanks and Boore, 1984) (Figs. 17 and 18).

5.3 Well log lithology

Water well logs from the Nevada Division of Water Resources were compiled into a database of underground lithology. The well logs were located and filtered based on quality and then divided into nine units based on the interpreted grain size. The database contains 1283 wells and covers the metropolitan area of the city of Pahrump and parts of central Pahrump Valley (Fig. 12, Appendix 2). The well log lithologies show a past playa and alluvial depositional environment. The logs contain fine-grained clay sediments, assumed to be from playa deposition in the northern central Pahrump Valley basin. Coarse-grained sediments located on the margins of the playa sediments are deposited from alluvial processes. Well logs located at the interfaces between the two domains have interleaving of both fine grained and coarse grained sediments.

CHAPTER 6

INTERPRETATIONS

6.1 SFS Fault Motion

The sense of motion of the SFS in Stewart Valley is observed as mainly

dextral strike-slip with a small component of normal dip-slip motion locally. The

strike-slip motion is evident from the (1) observed low vertical offset seen in

Saldaña (2009), (2) presence of a flower structure arrangement of fault traces in

the southwest trench, and (3) observed dextral wash offsets (dePolo et al., 2003;

Guest et al., 2007). The seismic data from Saldaña (2009) shows very little

normal displacement of interpreted sediment horizons across the trace of SFS.

This lack is consistent with a largely strike-slip motion fault.

The presence of the flower structure (tulip) in the southwestern trench (faults

C1-C8) indicates that even though there is mainly strike-slip motion along the

SFS, the trench site locations also contain a small component of extension and

normal-slip motion. This is most likely the result of a releasing bend in the fault

surface near the trench log site. Releasing bends are transtensional features

resulting from a bend in a fault that causes local extension during along strike-

slip.

Observed dextral offset of channels as described in Guest et al. (2007) is also

visible in the aerial photography and the field. Guest et al. (2007) discussed the

fault motion and inferred an offset from dated igneous rocks. Guest et al. (2007)

interpreted the Black Butte deposits and Devil Peak intrusion as a single magmatic event. The units, derived from volcanic and avalanche deposits, show offset of 30 ± 4 km since 13.1 ± 0.2 Ma (Guest et al., 2007). This yields a rate of 2.3 (± 0.35) mm/yr of slip during the Miocene and later. This offset is not consistent with current geodesic observations from Wernicke et al. (2004) and Bennett (1999) of ~1 mm/yr for the Stewart Valley region. This difference may indicate that: the fault is building stress before a future earthquake; the fault may be transferring slip onto another nearby fault such as the West Spring Mountain fault, East Nopah Range fault or the W166F; or the fault slip rate is slowing. Supporting the possibility of slip transfer/strain partitioning is the change of fault scarp morphology from the large height scarps observed in the southern and central Pahrump Valley to very small scarps in Stewart Valley. This change in scarp height is evident in the measured scarp profiles of Stewart Valley progressing from the south of Pahrump Valley northward into Stewart Valley and toward Amargosa Valley (Figs. 7, 8, and 9). The change in scarp height is evidence of change in the overall slip sense on the SFS. This change may be the result of dip-slip motion transferred through the partitioning of fault motion from the SFS to the WSMF, which is a normal fault (Fig. 12C).

6.2 SFS Continuity

The SFS has a surface that is continuous through Stewart Valley. This continuity is shown through a combination of seismic data, aerial photography, geologic mapping, paleoseismic trenches and topographic profiles. The presence

of the SFS in seismic data, trenches, and scarp profiles shows that in Stewart Valley, from northern Pahrump Valley to near the southern end of Amargosa Valley, the SFS is a continuous young dextral fault system with a very low component of vertical throw. The trench surveys and the pseudo 3D seismic study performed by Saldaña (2009) show that the SFS exists at a depth of at least ~50 m and ruptures to the surface in both northern and southern Stewart Valley.

The linear mesquite grove growth pattern in Stewart Valley is influenced by the number, size and locations of the fault strands. These strands are present in the trench and the seismic survey interpretations, and both align with the east playa mesquite grove that is visible in the aerial photography (Fig. 3). This grove extends from the south of Stewart Valley along the east margin of the valley playa to the north entrance of Stewart Valley (Fig. 3, Plate 1). It is most likely that this grove is taking advantage of the broken soil and fluid conduit of the fault and follows the fault traces as the fault extends through the valley.

Possible splays of the SFS in the Pahrump Valley

In the Pahrump Valley, two Quaternary fault systems are defined. The southwestern side of the Pahrump Valley is dominated by the SFS. The eastern side of Pahrump Valley is bordered by the West Spring Mountains fault (WSMF). The WSMF is a N-striking, W-dipping normal fault with a right-lateral oblique component in the south and mostly dip slip toward the north (Fig. 1)..

West Spring Mountains Fault and W116 Fault

The WSMF flanks the eastern Pahrump Valley (Fig. 1). The fault has a scarp, which is visible along the northeastern and east-central valley border with smaller discontinuous scarps in the south. The 11-km-long central segment contains a single scarp that is at one point is 9.4 m high (Anderson et al., 1995). Based on scarp profiles, the WSMF scarp displays two events (Anderson et al., 1995) (Fig. 17). Using soil diffusion modeling the youngest event is estimated to be Pleistocene or early Holocene in age with a maximum fault displacement estimated at 5 m, which suggests an event of M6.5-7.4 occurred to form the scarp (Anderson et al., 1995).

Workman et al. (2008) and Hoffard (1991) suggest that the WSMF is a splay of the SFS. Anderson et al. (1995) state that the WSMF is connected to the SFS (which they refer to as the Pahrump-Stewart Valley fault-"PSV"). On the central segment, Anderson et al. (1995) state the motion of the WSMF is dip-slip, but that the en echelon stepping arrangement of the southernmost extent of the WSMF scarps in the central Pahrump Valley implies some component of lateral movement that is being accommodated through scissor faults (Anderson et al., 1995).

Using data analysis of the well logs, air photos, previous maps by Workman et al. (2008) and Hoffard (1991), and field observations, it is possible to document the 3D architecture of the basin-fill sediments and basin structure through abrupt changes in sedimentary facies. 3D modeling of the lithology and depositional environments of shallow basin fill improves the understanding of

fault location, type, offset, and surface rupture length. 3D basin models, derived from well log lithology, depict the locations of fault surfaces by showing abrupt changes in units and unit offsets among multiple wells (Fig. 12). As displayed in the 3D representation of the well log sediments, the lithologic data show a depositional environment dominated by interfingering alluvial deposits of coarse material (gravel and sand) and fine grained sediments (clay and soils). This interfingering nature is best displayed in the well log cross section B to B' across the southern Pahrump Valley away from any faults that could offset the sediments (Figs. 12 and 19). These playa sediments in the northwestern Pahrump Valley exhibit right-lateral displacement of 10 km, consistent with the motion sense of the SFS. The offset fine-grained sediments show abrupt changes in grain size with no interfingering due to the tectonic offset rather than depositional emplacement of the sediments as seen in the southern well log cross section (Figs. 12 and 19). This assumes that the fine-grained sediments are originally deposited as an oblate semicircle in map view. The 10 km offset distance is determined from the needed amount of along fault strike offset to return the offset fine grained sediments to the original oblate semicircle (Figs. 12 and 19).

The orientation of W116F, dextral motion of W116F, the dextral motion of the SFS and the orientation and normal slip of the WSMF in Stewart Valley imply that the WSMF and W116F are likely accommodating strain partitioning along the east side of the Sierra Nevada and western CBR. The deformation is from the dextral slip of SFS, which is at an oblique angle to the Pahrump Valley resulting

41

in motion along both W116F and the southern section of the WSMF in a dextral and normal sense (Figs. 6 and 1). When comparing the SFS fault scarps to the WSMF scarps there are two changes in slope angle that appear to be common to both scarps. This would indicate similar ages of faulting and perhaps strain partitioning or slip transfer. The Pahrump basin could not have formed from this process alone. This is due to the inability of pull-apart basin formation to cause the magnitude of relief of the Spring Mountains and the Last Chance mountain range although it is a likely a contributing factor to the more modern basin development. This multiphase basin development for the Pahrump Valley is previously described in Scheirer et al. (2010). Scheirer et al. (2010) examines the Pahrump and Mesquite basins using geophysical techniques to describe the current and past basin development. The Scheirer et al. (2010) description of Pahrump and Mesquite basins aid in showing both (1) an initial extensional phase of basin development and then a strike slip phase of development and (2) that the Mesquite and Pahrump basins are linked by the strike-slip motion of the SFS.

6.3 Earthquake Hazard

The SFS poses an earthquake risk for the developed regions of Pahrump and Las Vegas. The surface rupture length, the relatively young dates of earthquake occurrence, the presence of reoccurring earthquakes, and the implied large displacement of the past earthquakes establish a significant earthquake risk to the southern Nevada and California region.

6.3a Surface Rupture Length

The surface rupture length of the SFS is 150 km starting near Primm, Nevada continuing north into the Pahrump Valley southwestern margin, extending to through Stewart Valley (Hoffard, 1991; Guest et al., 2007; Chapter 5.2), and northward into the Amargosa Desert region (Donovan, 1991; Guest et al., 2007). As suggested by Donovan (1991) and Guest et al. (2007), the SFS may continue underneath the relatively young and poor fault scarp preserving sediments of the Amargosa Desert and Crater Flat region to Bare Mountain near the town of Beatty, Nevada making the total potential length of the fault rupture 200 km. The length when compared to other instrumented earthquakes having documented surface rupture lengths implies that the SFS could host a possible M7.6 to M7.7 earthquake (Wells and Coppersmith, 1994) (Fig. 14). The surface rupture length of just the Pahrump segment of the SFS is 35 km, which includes the Stewart Valley section. This distance is measured from the scarps of the SFS that are in the south of the Pahrump Valley to the northern trench site and topographic and bedrock change entering into Amargosa Valley at the north end of the Stewart Valley. Using the Wells and Coppersmith (1994) surface rupture length vs. earthquake magnitude correlation, the Pahrump segment of the SFS would support a M6.9 earthquake (Fig. 14).

The SFS is shown to be a continuous feature in Pahrump and Stewart valleys using the trench data, scarp data and surface features, however, the SFS may not rupture across its whole length during an earthquake. The north and south

trench site data and the scarp bevel data imply that although multiple

earthquakes have occurred, the correlation of specific events is not possible

(Figs. 8, 9, 17, and16, Plate 1). There is a possibility that the SFS may not

rupture as an entire unit. This is important because the magnitude of an

earthquake on just the Pahrump segment is still a significant hazard to the

Pahrump and Las Vegas developed regions.

6.3b Earthquake events

The SFS fault shows recent, large motion earthquakes interpreted from the

trench log data, scarp profiles, and the ^{14}C ages of the sediments in the trench.

The SFS had at least three, or possibly four, earthquakes that formed surface

ruptures with offset of the sediment layers in the fault trenches (Fig.16). The

dated offset sediment horizons when bracketed with dated younger undisturbed

horizons yield windows of time during which two of the fault-forming earthquakes

occurred (Fig. 10). The data from the trench logs show that an earthquake

occurred before deposition of unit 4 and another occurred before the deposition

of unit 3 (somewhere around 3340 and 8640 cal yr B.P) (Plate 1). The two

younger earthquakes are shown by faults that end within (1) lower unit 2 and (2)

upper unit 2. Although trench scarp profiles and locations of the fault splays in

trench supports an interpretation of 3 events, there remains the possibility that

the two fault sets that end in unit two were created by a single event. Due to

overlap in the uncertainty of the dates of the samples taken in unit 2, if two

events occurred they cannot be distinguished in time. This overlap implies a

single event occurring between 1060-560 cal yr B.P., or 2 separate events

occurring between (1) 3340-560 cal yr B.P. and (2) younger than the samples

SWT012 (1060 – 930 cal yr B.P.) and SWT011, which yielded a contaminated

date of 1956 AD (Fig. 10, Appendix 1). Faults J4 and II offset units

stratigraphically higher than the other faults. This may be indicative that the fault

strands are result of a separate younger event than the other fault surface

forming events. These dates demonstrate that the fault experienced recent

activity and the fault experiences recurring earthquakes. The radiocarbon dates

of the sediment horizons cut and uncut by fault surfaces also overlap for the

sampled site from the southeastern trench and the southwestern trench. This

reinforces the interpretation that an earthquake occurring between 680-560 cal yr

B.P. and 1060-930 cal yr B.P. ruptured fault surfaces in both trenches as one

event. This event would be separate from the fault ruptures observed in the north

trench log where a single uncut sediment horizon radiocarbon date implies that a

separate earthquake occurred before unit 3 and another before unit 4. The data

show three recent events occurred on the SFS two of which occurred in the last

1060 cal yr BP and all three of which most likely occurred 3240 – 3210 cal yr BP.

    The bevels in the SFS and WSMF scarp profiles also show that multiple

events occurred in recent history. In order to form a fault scarp with bevels,

relatively large earthquakes had to have occurred with enough energy to form a

steep fault scarp surface more than once. A fault scarp can preserve each event

as a separate bevel. Each bevel is exposed to erosion for different amounts of

time until the scarp profile erodes to become curvilinear when viewed as a

topographic profile perpendicular to the fault scarp strike (Fig. 13). The number of bevels can then be correlated to the number of events that have occurred and have not had enough time to erode. The north trench profile (Fig. 7) is a profile that contains four bevels possibly recording four separate events. The north point fault scarp profile (Fig. 7) has three distinct bevels and may have had three events occur on the fault. The south road total station transect (Fig. 7) has four bevels and four events. The scarp profiles in the north of Stewart Valley show less than 5 m relief indicating that the SFS in this region is mainly strike-slip (Figs. 7 and 9). The South trench profiles #1 and #2 when overlaid onto each other show four bevels and four events (Fig. 8). The loop road profile shows three distinct bevels representing three events have occurred (Fig. 8).The south Stewart Valley scarp shows erosion from a transecting wash in the middle of the profile but the undisturbed portions of the scarp may have two bevels present (Fig. 8). The scarps in the south of the Stewart Valley progressing northward have less relief, which may be indication of a change in fault slip direction from an oblique normal component slip to a pure strike-slip motion (Figs. 7, 8, and 9). The WSMF fault scarps show two slope changes and bevels indicating two scarp-forming events have occurred in the recent past of the WSMF (Figs. 17 and 18). The data from the fault scarp profiles measured on the SFS show that possibly three to four fault scarp-forming events have occurred recently enough that erosion has not erased the profile bevels. Although the magnitude of the bevels varies greatly on the SFS, at least two distinct bevels occur. A possible

third bevel is present in both scarps observed in the southern and northern extents of Stewart Valley.

6.3c Past Large Magnitude Events

The data in this study support the conclusion that the SFS had past large magnitude earthquakes. This conclusion results from the overall length, presence of fault scarps and the presence of faults surfaces and liquefaction features in the trench.

Liquefaction features are diagnostic of large shaking due to the required high shaking threshold needed to form the features. Liquefaction features are the result of the transformation of a saturated granular material from a solid state into a liquefied state because of increased pore-water pressure (Youd, 1973). Liquefaction indicates that an earthquake of a large enough magnitude occurred to mobilize lower sediments allowing them to intrude into the overlying host sediments. The threshold horizontal acceleration to form a liquefaction feature is approximately 0.2 g for strong earthquakes in highly susceptible sediment (National Research Council, 1985; Ishihara, 1985). Historical records demonstrate that in order to form a liquefaction feature the typical earthquake must be of a magnitude of at least M5 but liquefaction features are more common in magnitudes of at least M5.5-M6 (National Research Council, 1985; Ambraseys, 1988). This implies that an earthquake of at least M5 has occurred on the SFS or a stronger nearby earthquake has occurred nearby. (National Research Council, 1985).

The presence of liquefaction features in the trench indicates that a large magnitude earthquake occurred in the past on the SFS. The stratigraphic locations of the liquefaction features (Plate 1) imply that the liquefying events in both south trenches occurred after the emplacement of the 1060-560 cal yr B.P. radiocarbon dated sediment of unit 2.

It is important to note that liquefaction is an indicator for the Modified Mercalli index, a commonly used qualitative scale of seismic effect by Wood and Neumann (1931). This system is used in rating seismic effects from I to XII gauging barely felt earthquakes to complete devastation. The scale places a threshold of liquefaction at intensity VI. Intensity VI is generally defined as an earthquake "Felt by everyone, being difficult to stand, with some heavy furniture moved, plaster falling and chimneys may be slightly damaged."

The presence of liquefaction features in Stewart Valley suggest that structures and infrastructure in Stewart and Pahrump valleys should be inspected to establish if liquefaction is a risk needing mitigation in future construction and retrofitting existing facilities. Both Stewart Valley and Pahrump Valley have similar fine-grained sediments in parts of them. If the water table is shallow and an earthquake occurs in a similar way that caused the liquefaction as seen in Stewart Valley, liquefaction could also occur in Pahrump Valley near and around the city of Pahrump, resulting in damage to the buildings and infrastructure.

6.4 Relationships between Strike-Slip and Extensional Faults

The SFS lies at the overlap of the CBR, Walker Lane Belt and ECSZ. Geographic location and strike-slip motion define the ECSZ and Walker Lane Belt. The two systems are very similar. The overlap of the two fault systems also coincides with the defined west margin of the CBR. The CBR contains north-striking extensional faults and northwest-striking right-lateral faults. The interface between these two fault types lies near the SFS and Pahrump Basin.

The SFS has characteristics that may relate to the interface of the western CBR strike-slip faults (ECSZ and Walker Lane Belt) and the eastern extensional faults. The interface is defined by changes of fault slip sense. The Pahrump Valley contains the SFS and W116F, interpreted as a splay of the SFS (Fig. 12). The slip sense of these two faults is dextral. The WSMF is a fault system on the eastern margin of the Pahrump Valley (Fig. 12). The WSMF shows mainly dip-slip motion in the north and central sections of the fault zone. The southern section shows en echelon splays (Fig. 12). The southern section of the WSMF accommodates oblique-slip while the central and north sections of the WSMF appear to have dominantly dip slip. This change in slip may be due to influence from the W116F. The W116F is interpreted to accommodate the lateral component of that slip evident farther south on the southern section of the WSMF. The orientation of the WSMF and W116F, and the change in slip sense along the WSMF suggest that some strike-slip is accommodated on the southern part of the WSMF while the central and north sections of the WSMF and the W116F are partitioning the SFS motion (Fig. 12). This suggests that the interface

49

between the extensional faults to the east of the CBR and the strike-slip faults to the west is likely in the Pahrump Valley. This interface is important because it shows the location of where the extensional faults of the eastern CBR meet the strike slip motion of the ECSZ, Walker Lane belt and the western CBR. Consequently, these faults lie near the interface of the extensional tectonic regime to the east and the plate boundary-influenced strike slip to the west.

CHAPTER 7

CONCLUSIONS

Using the radiocarbon ages of soil and sediment horizons that are cut by fault

ruptures of the SFS, it has been determined that the SFS poses a significant

hazard to the southern Nevada and southeastern California region. The results

show that the SFS had earthquakes in the recent past. The paleoseismic trench

study shows radiocarbon ages that define at least three and possibly four unit

offsetting earthquakes. Three of these events occurred since ~ 3300 cal yr B.P.

One event may have occurred as recently as 1060 cal yr B.P.

The SFS had strong motion earthquakes in the recent past. The presence of

liquefaction features implies that an earthquake of greater than M5 occurred in

the past. The multiple offsets of the sediment horizons recorded in the trenches

indicate past earthquakes with strong motion that ruptured the surface. The

overall length of the SFS, when compared to other faults with known magnitudes

and surface rupture lengths, indicates the possibility that a large magnitude

earthquake occurred on the SFS (c.f., Wells and Coppersmith, 1994). The fault

scarp bevels imply that at least two scarp forming events that occurred in recent

enough time to prevent erosion from erasing them.

The SFS is present and ruptures the surface in Stewart Valley. The trench,

aerial photos, and scarp topography profiles show the SFS exists at the surface

in both the north and south of Stewart Valley. The SFS influence is not confined

to the state line between the California and Nevada state border. The SFS has

an interpreted splay into the Pahrump Valley. This splay, W116F, is influencing

fault motion on the WSMF. Using well log lithology, it is evident that the SFS has a splay that passes through the city of Pahrump. Pahrump Valley may be a hybrid pull apart basin/normal fault basin involving the WSMF and the SFS. The orientation of the faults and motion direction results in strain partitioning of the extension and right-lateral strike-slip offset (Fig. 1). The extension and right lateral offset influences the basin development of the Pahrump Valley, forming a negative topographic feature.

The SFS is at the transition of western strike-slip faults and eastern extensional faults. The geographic location of the SFS is inside the overlapping regions defined for both of the Walker Lane Belt and the ECSZ and the CBR. The observed SFS rate of modern offset from geodesy, the SFS fault geometry, reoccurrence interval, and stick-slip motion of the SFS is similar to the ECSZ and Walker Lane Belt. The motion and en echelon stepping of the southern WSMF also indicate that a combination of normal and strike-slip motion occurring on the southern segment of the WSMF. Both of these faults may be at the margin between the western strike-slip faults and the eastern extensional faults in the CBR.
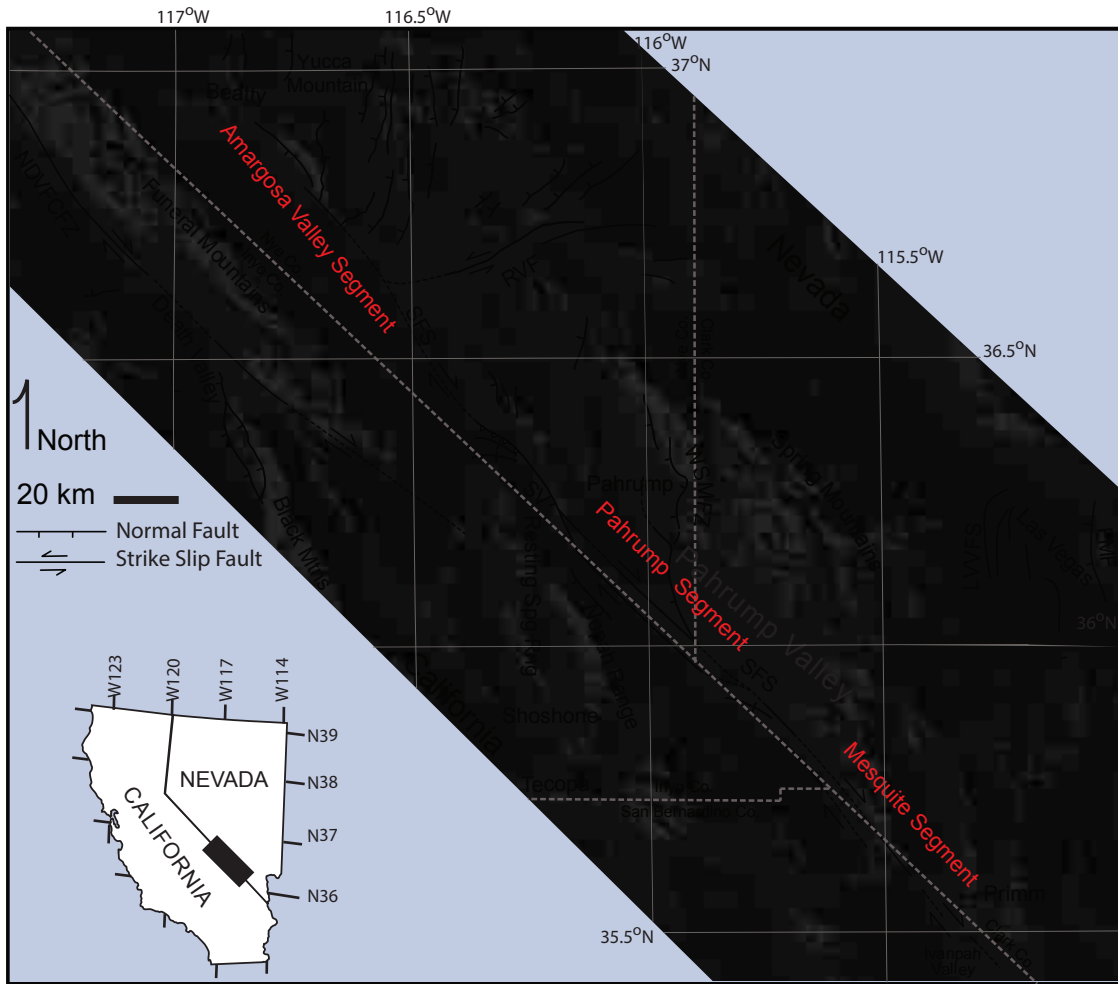
Figure 1. The Stateline Fault system (SFS) is composed of three fault segments: the Mesquite segment, Pahrump segment and Amargosa segment. Las Vegas Valley fault system-LVVFS, North Death Valley\Furnace Creek Fault Zone-NDFCFZ, Rock Valley Fault Zone-RVF, Stewart Valley SV, and West Spring Mountain Fault Zone-WSMFZ, Frenchman Mountain Fault-FMF. Fault locations are modified from Guest et al. (2007) .

Figure 2. Quaternary faults of the Central Basin and Range (modified from Fossett, 2005 and the USGS Fault and Fold Database). Stateline fault system in red. Dashed lines where faults are concealed. Arrow Canyon Range Fault (ACRF), Black Hills Fault (BHF), Black Mountains (BM), California Wash Fault (CWF), City of Pahrump Splay of the SFS (PAH), Death Valley (DV), Death Valley-Fish Lake Fault Sytem (FLVFS), Deep Springs Valley Fault System (DSVF), Eldorado Valley Fault (EVF), Frenchman Mountain Fault (FMF), Furnace Creek Fault Zone (FCFZ), Garlock Fault (GF), Las Vegas Valley Fault System (LVVFS), Mead Slope Fault (MSF), North Death Valley Fault Zone (NDVFZ), Nopah Range (NP), Owens Valley Fault (OVF), W116 Fault (W116), Panamint Valley Fault (PVF), Stateline Fault System (SFS), West Spring Mountains Fault (WSMF), White Mountains Fault Zone (WMFZ), Wildcat Wash Fault (WWF).
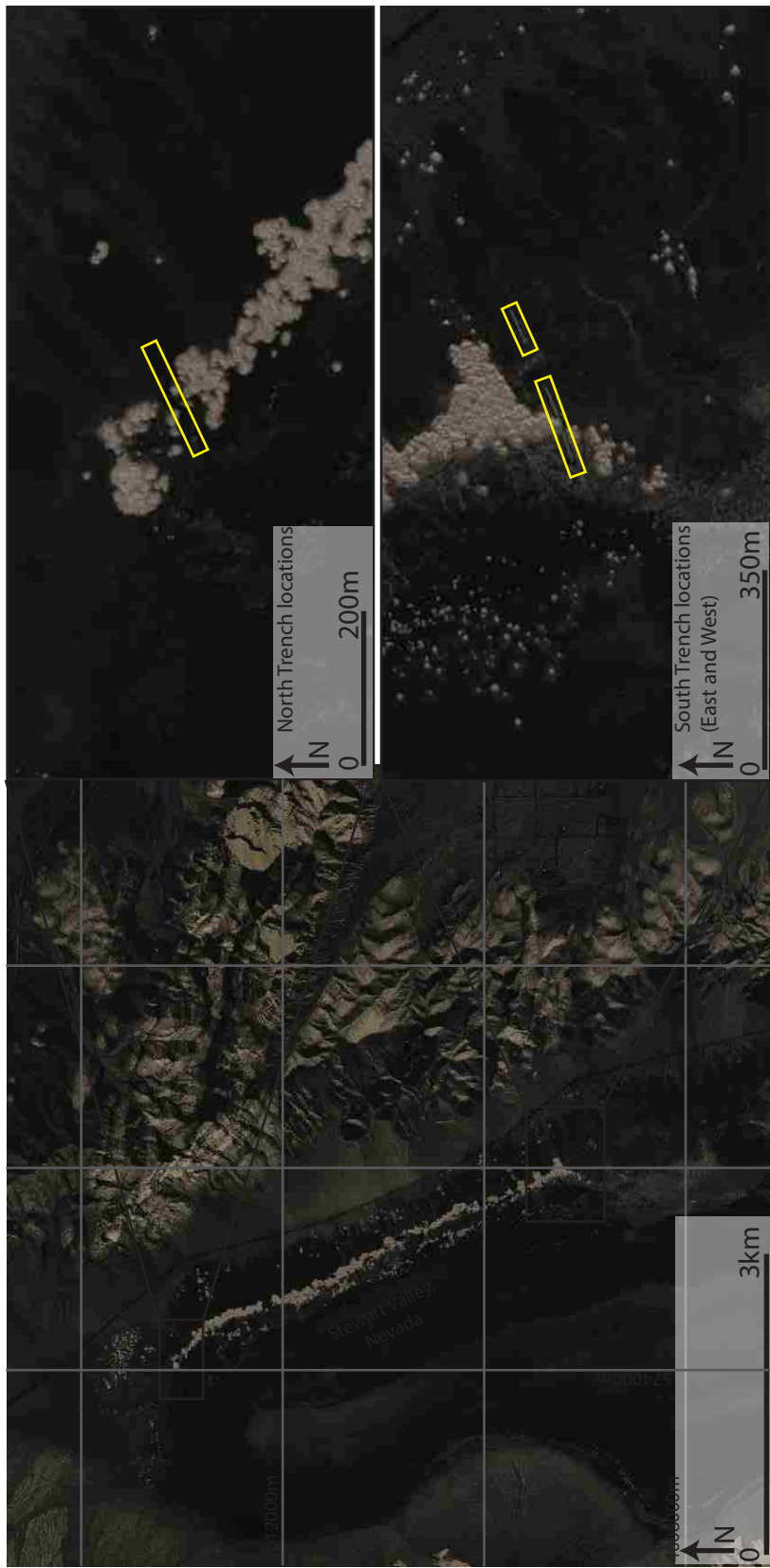
Figure 3. Trench site locations in Stewart Valley. Trenches were excavated in northern and southern Stewart Valley where the fault was previously interpreted to exist by geophysics and surface features (dePolo, 2003; Saldaña, 2009). Trench site locations are highlighted in yellow. Imagery taken from the National Agriculture Imagery Program (NAIP). Grid in UTM.
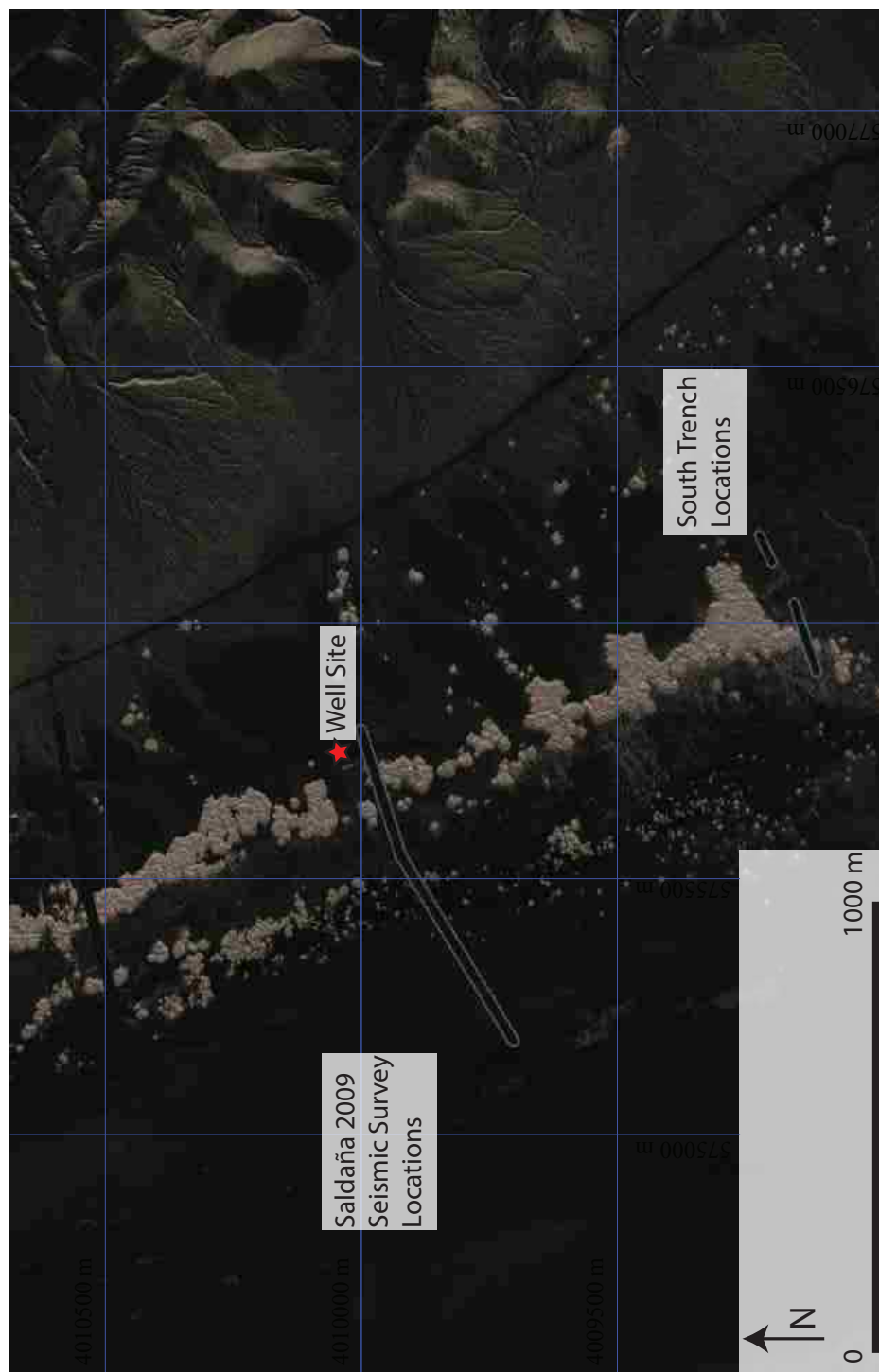
Figure 4. Seismic line locations in Stewart Valley. Aerial photograph from National Agriculture Imagery Program (NAIP) with the southern paleoseismic trench study site (red lines) and the seismic study of Saldaña (2009) (purple and orange lines) shown in relation to each other. The orange seismic study line called line 1 in Figure 5 was used to compare the SFS in relation to the southern paleoseismic trenches in Figure 5. The red star indicates the location of the well used to properly set the depth of the seismic study in relation to the surface and trench logs. Grid in UTM.
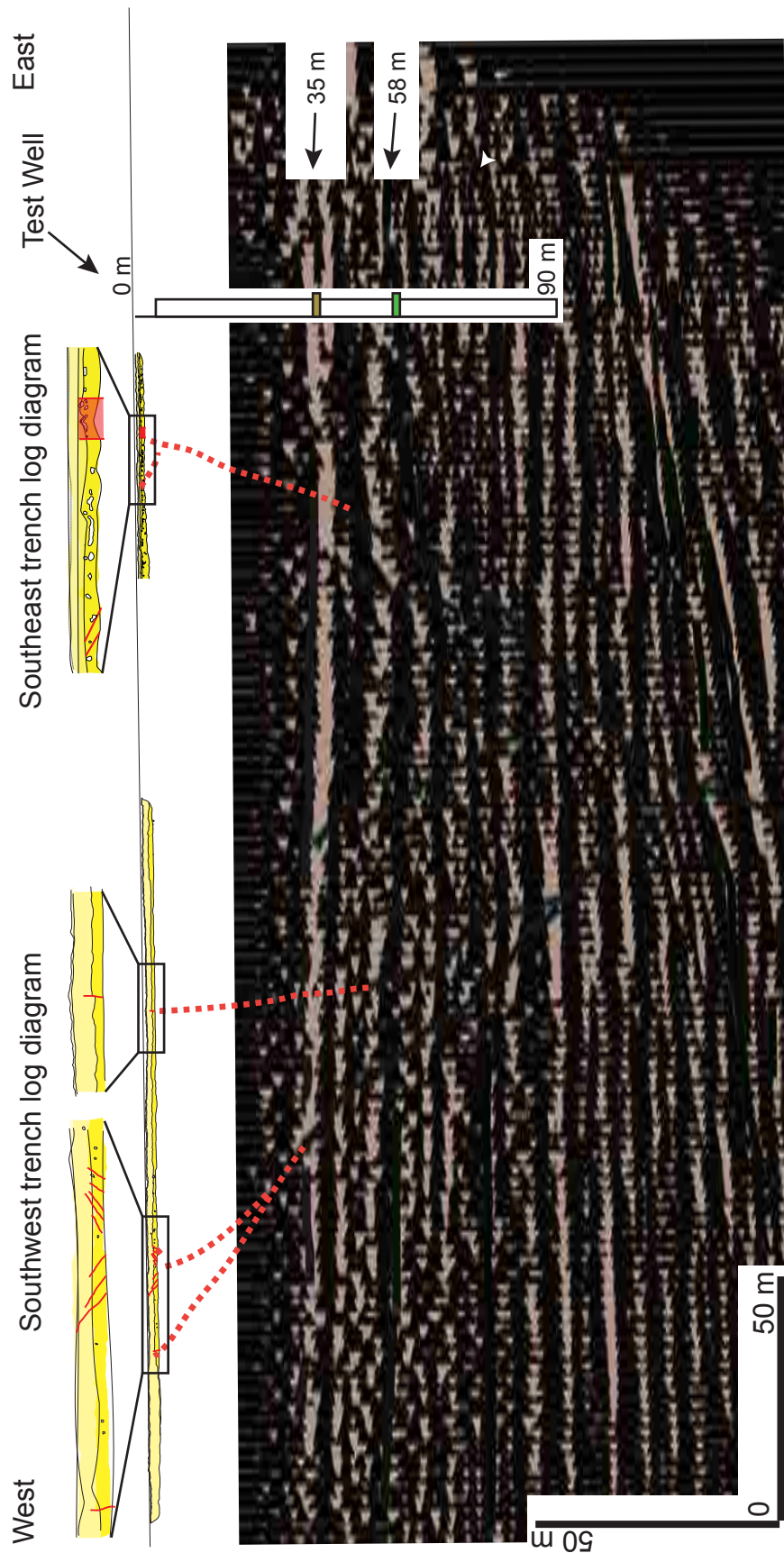
Figure 5. Trench Logs in relation to seismic reflection profile. Cropped seismic reflection from Saldaña (2009) and south trench logs. Line 1 superimposed at scale underneath the south Stewart Valley trench log diagrams. The relative altitude of trench log diagram is set using a nearby well log unit description and depth to a lithology type change that matches the first sets of seismic refectories of the seismic diagram. The trench log diagram is enlarged by 300% above the original scale trench to better show faults in trench. Red dashed lines indicate fault locations are approximate. Brown, purple, green, and blue lines are traced horizons interpreted by Saldaña (2009). Trench and seismic locations are located on Figure 4.
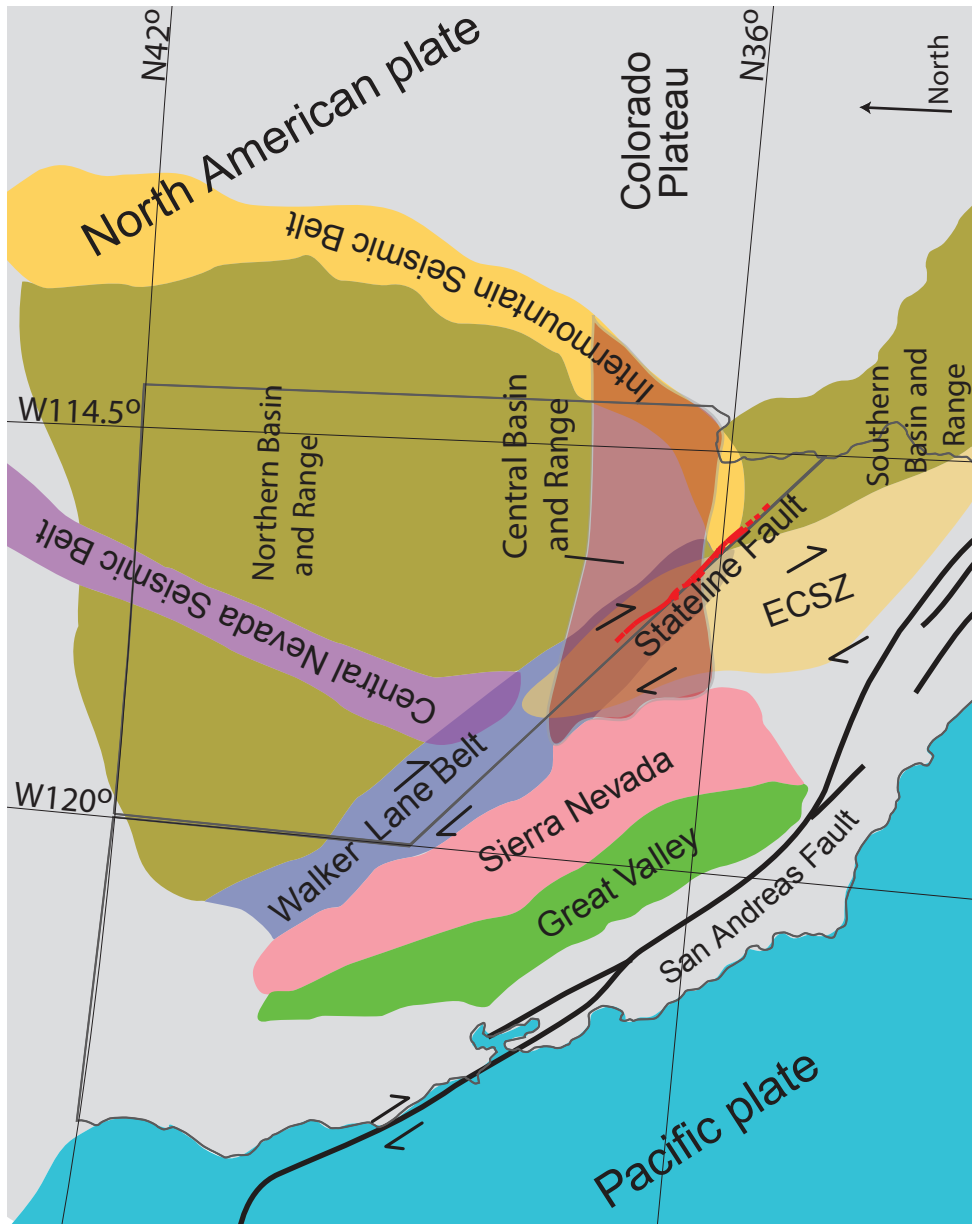
Figure 6. Regional tectonic domains. Generalized diagram of the southwest United States with the SFS highlighted in red to show relationship to the regional tectonic domains. Arrows show general tectonic motion. Domains are defined in Chapter 1.3.

Figure 7. Stewart Valley fault scarp locations. Multiple sites along lineations and known scarps were surveyed using a TOPCON Robotic Total Station to build topographic profiles for analysis. Transect locations are marked in red lines. UTM grid shown. Modified image from Google Earth. Profiles are shown on Figure 7 and Figure 8.
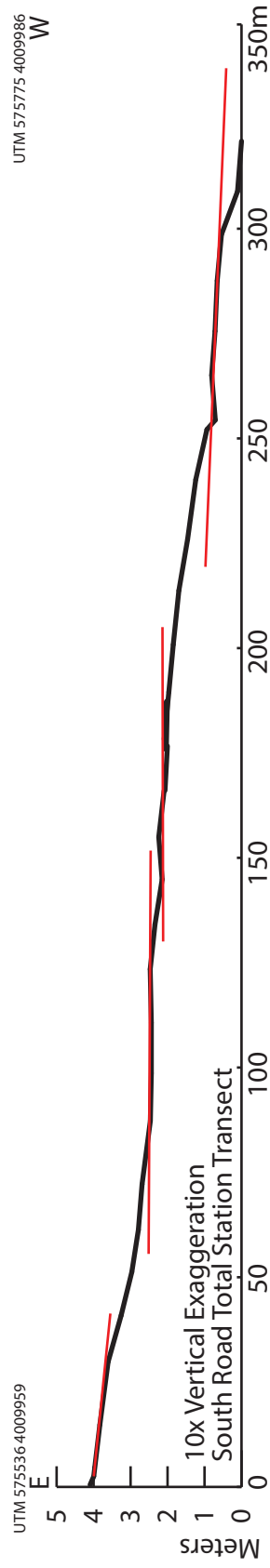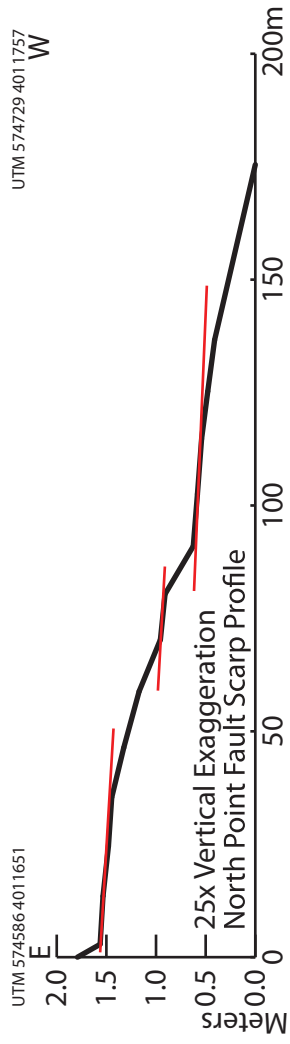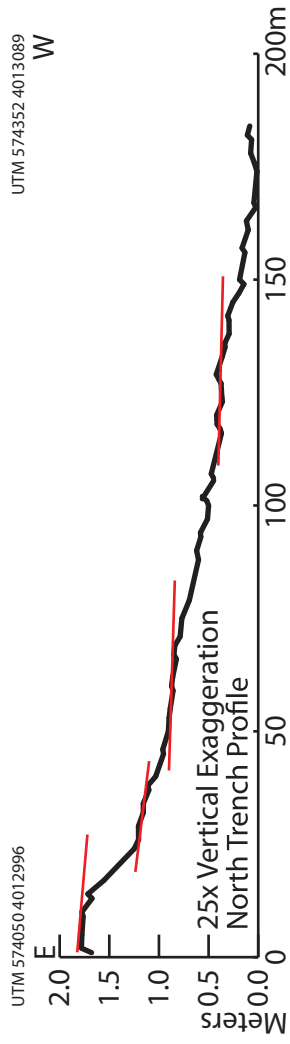
Figure 8. Topographic profiles of central and northern Stewart Valley. The red lines highlight the slope gradient with breaks caused by the occurrence of multiple scarp forming events. Profile locations are plotted on Figure 7.

W

UTM 576348 4009344

8.5x Vertical Exaggeration
South Trench Profiles #1 and #2

UTM 575703 4003991

E
8
7
6
5
4
3
2
1
0

Meters

W

UTM 579144 4003652

8.5x Vertical Exaggeration
Loop Road Profile

UTM 578971 4003529

E
8
7
6
5
4
3
2
1
0

Meters

W

UTM 580640 4002859

3x
Vertical
Exaggeration
South Stewart Valley Fault Scarp Profile

UTM 580521 4002726

E
20

15

10

5

0

Meters
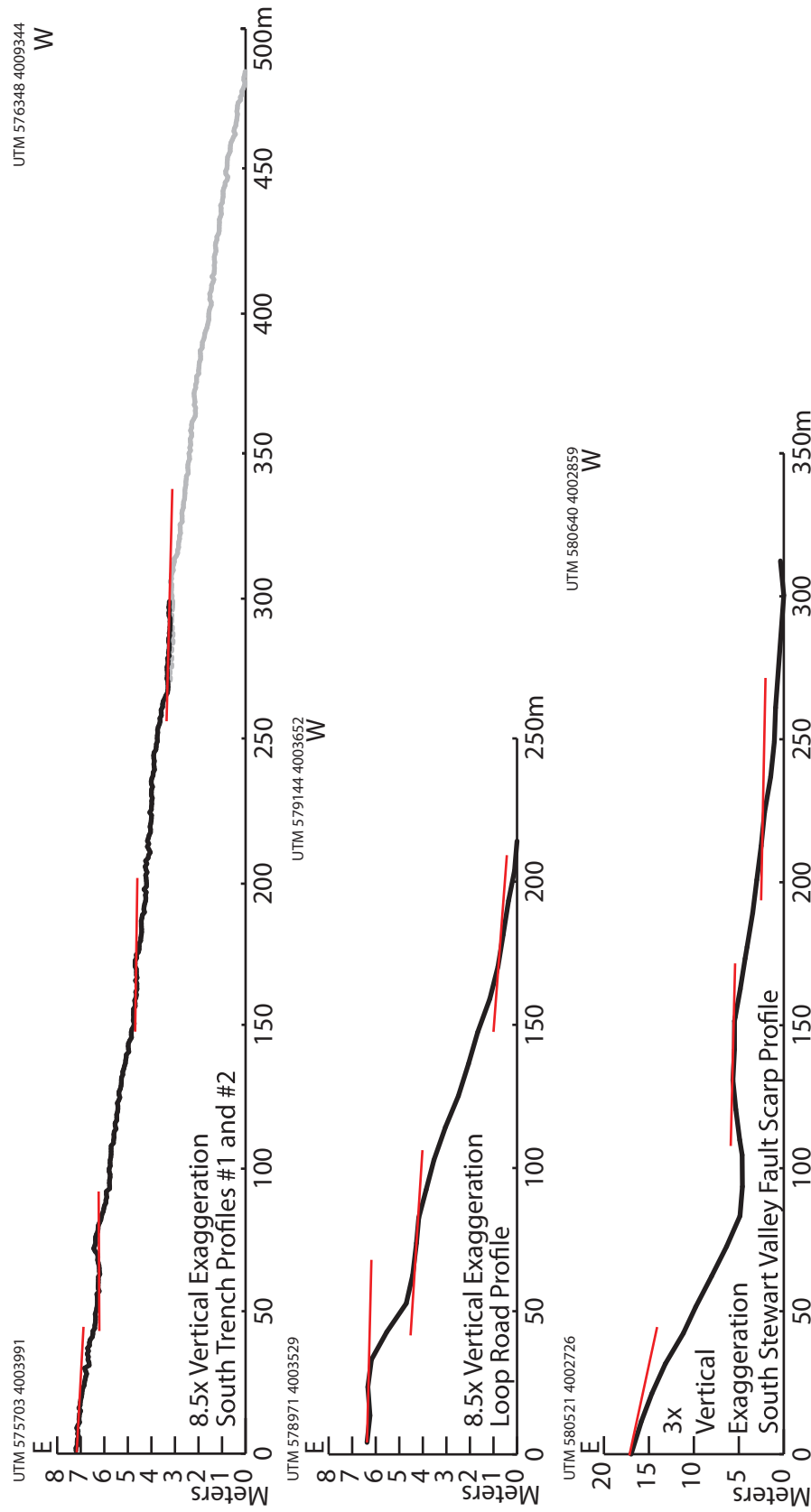
Figure 9. Topographic profiles of the southern Stewart Valley Fault scarps. The red lines highlight breaks in the slope gradient caused by the occurrence of multiple scarp forming events. South Trench Profiles is a composite of two parallel profiles aligned perpendicular to the SFS strike. Profile locations are plotted on Figure 7.

61
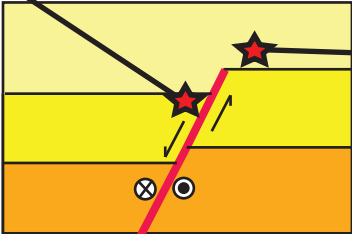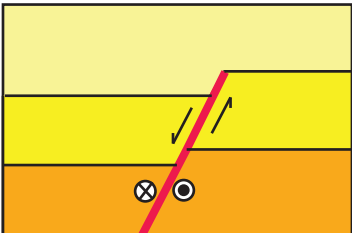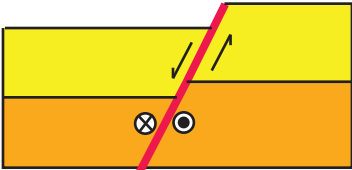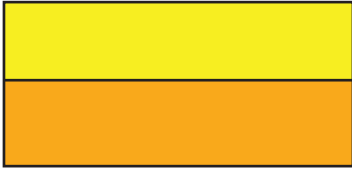
Sediments as seen in cross section	Description of sediment interaction	Time
Oldest age / Youngest Age / Fault	Using the radiocarbon age of the cut and uncut sediments near the fault tip, the earthquake can be bracketed to have occurred after the deposition of the cut beds and before the deposition of the uncut bed.	Modern
Fault	New sediments are deposited and bury the fault.	
Fault	An earthquake occurs. The resulting fault cuts through the sediments to the exposed surface.	
	Newer sediments are deposited	
	Initial sediment deposition	Older

Figure 10. Fault dating from offset sediments. Diagram showing the relationship between cut and uncut sediments and how sampling can bracket the age of a fault surface.
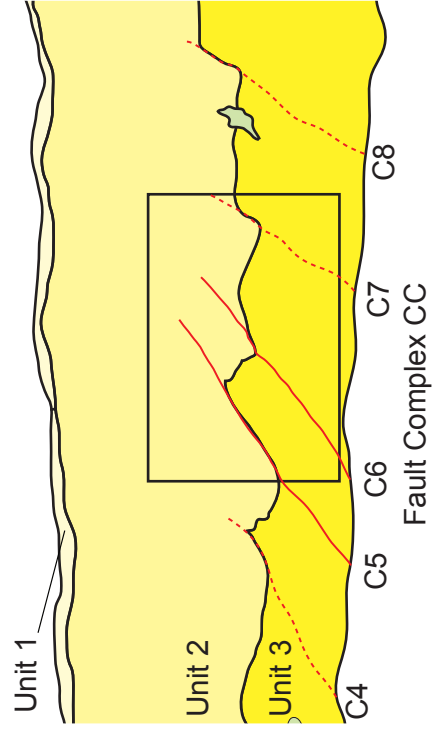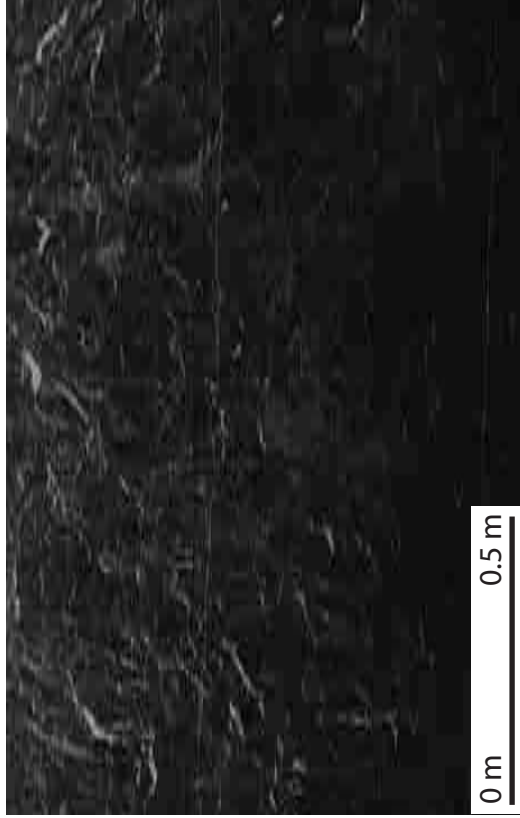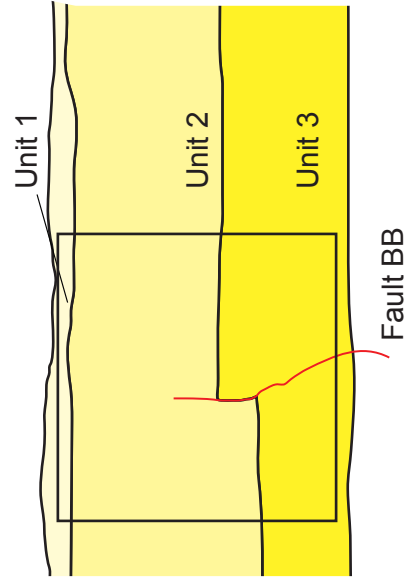
Figure 11. Photos of trench showing offset of units by fault surfaces. Unit 2 and 3 contact marked by orange colored nails. Faults marked by yellow and blue nails. Trench log interpretation beneath. Faults lined in red. Liquefaction in grey. Photo location in black.
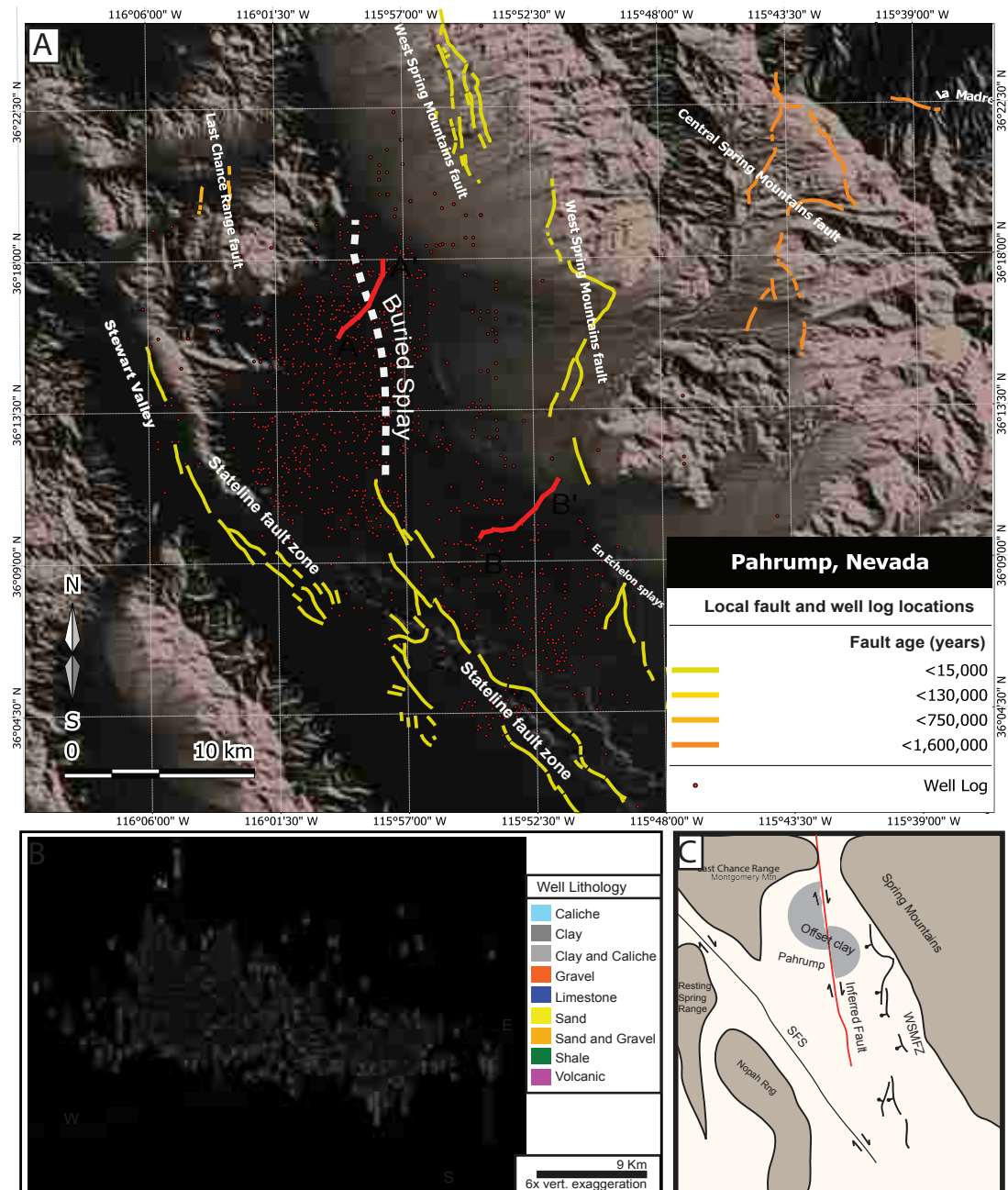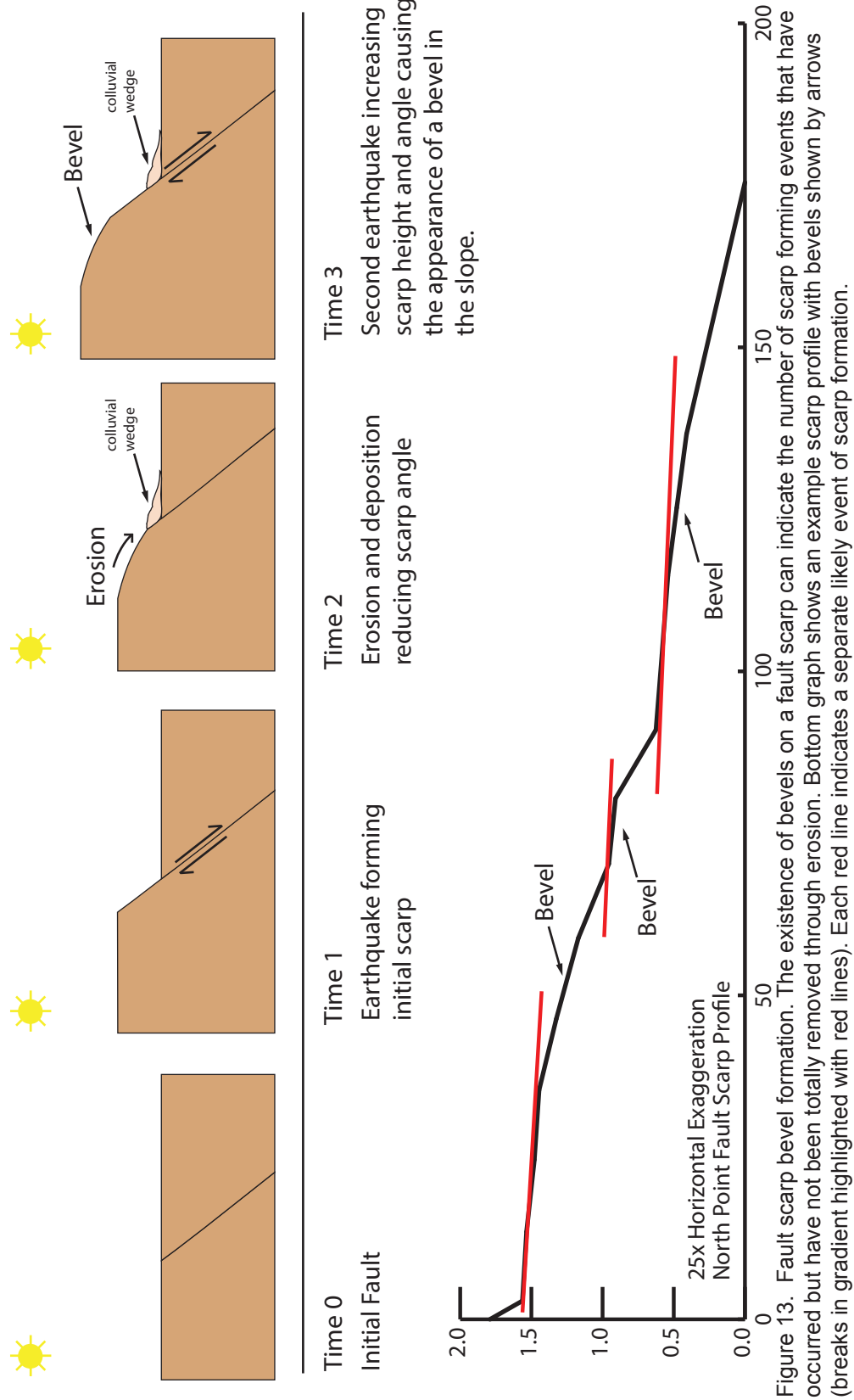
Figure 12. Pahrump well log locations. A. Locations of water well log sites and locations of known local faults from the USGS Fault and Fold Database in Stewart and Pahrump valleys. Fault splay located using offset grain sizes in well log sediments in white dots. Well log cross-section transect locations shown on Figure 16 in red. The locations of the well log cross sections were placed both across the inferred fault location (A-A') and away from any known faults to show contrast between the depositional and tectonically controlled sediment configurations in the well logs. B. 3D well log construction showing the fine grained pluvial sediments (grey) in relation to the coarse grained alluvial sedments (yellows and oranges). Note the offset of the fine grained grey units.C. Conceptual diagram showing relation of fault splay and offset fine grained sediments. Orientation of WSMF and inferred splay are preferential to strain partitioning of SFS fault strain.

Time 0
Initial Fault

Time 1
Earthquake forming initial scarp

Time 2
Erosion and deposition reducing scarp angle

Time 3
Second earthquake increasing scarp height and angle causing the appearance of a bevel in the slope.

Bevel

colluvial wedge

Erosion

colluvial wedge

Bevel

Bevel

Bevel

Bevel

2.0
1.5
1.0
0.5
0.0

0   50   100   150   200

25x Horizontal Exaggeration
North Point Fault Scarp Profile

Figure 13. Fault scarp bevel formation. The existence of bevels on a fault scarp can indicate the number of scarp forming events that have occurred but have not been totally removed through erosion. Bottom graph shows an example scarp profile with bevels shown by arrows (breaks in gradient highlighted with red lines). Each red line indicates a separate likely event of scarp formation.
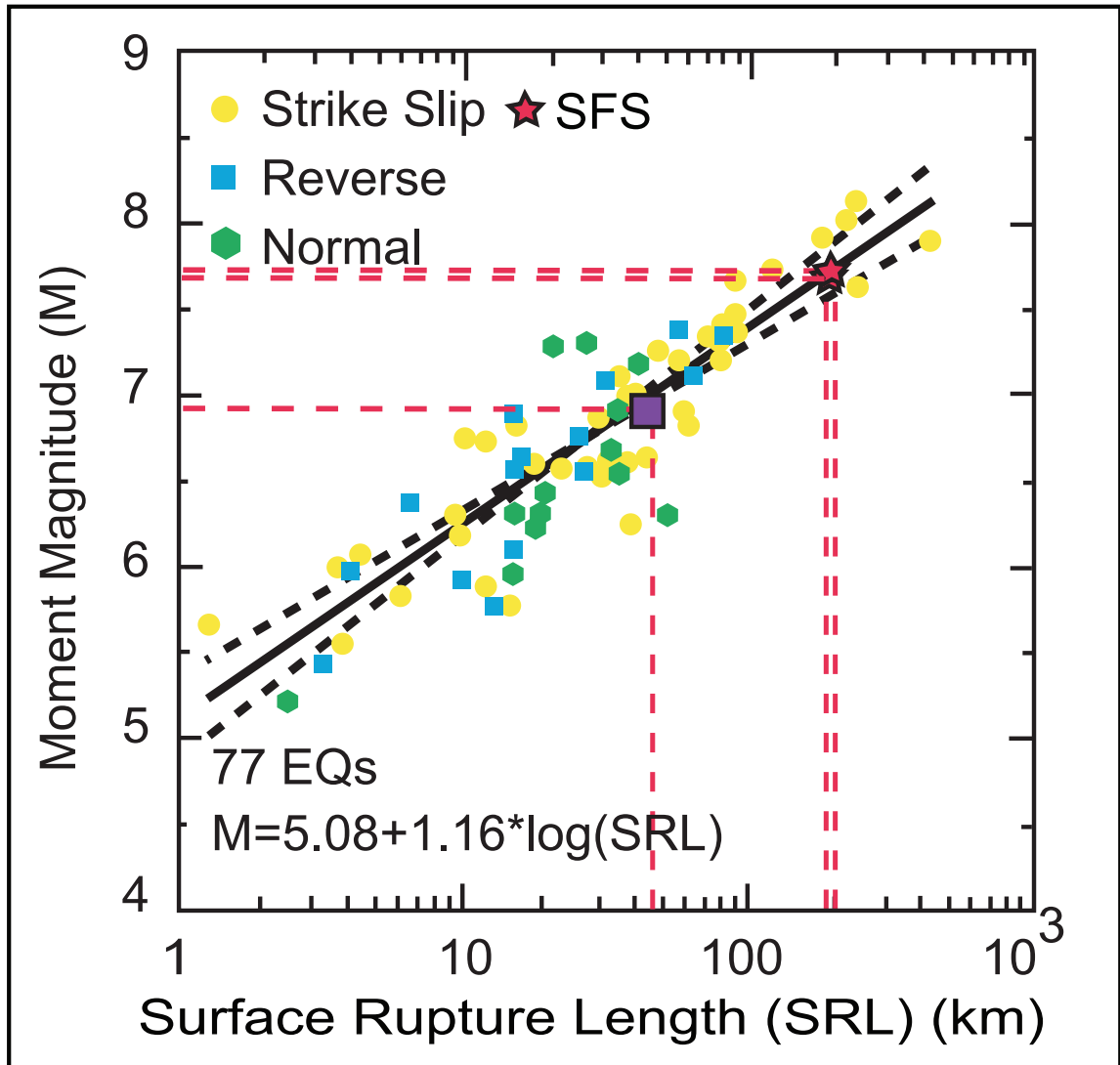
65

Figure 14. Surface ruptures lengths vs. possible earthquake magnitudes. Graph of instrumentally recorded earthquake data plotted by Wells and Coppersmith (1994) showing the correlation between the surface rupture length of a fault and earthquake magnitude. Data from the estimated maximum SRL on the SFS was added. The resulting magnitude from the two different lengths of the SFS overlap on the graph. The smaller length results in a M7.6 and the larger length results in a M7.7 earthquake. The purple square signifies a rupture on only the Pahrump Segment of the SFS running 35 km in length and resulting in a M6.9 earthquake.
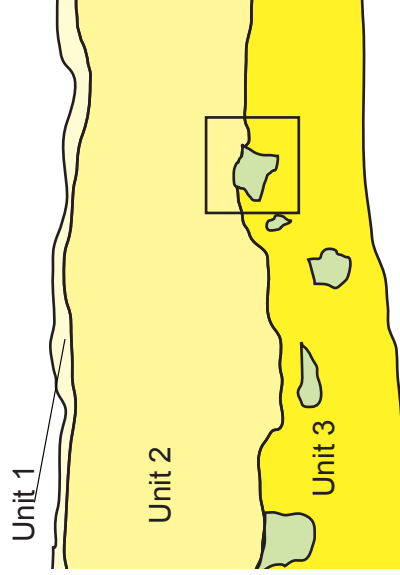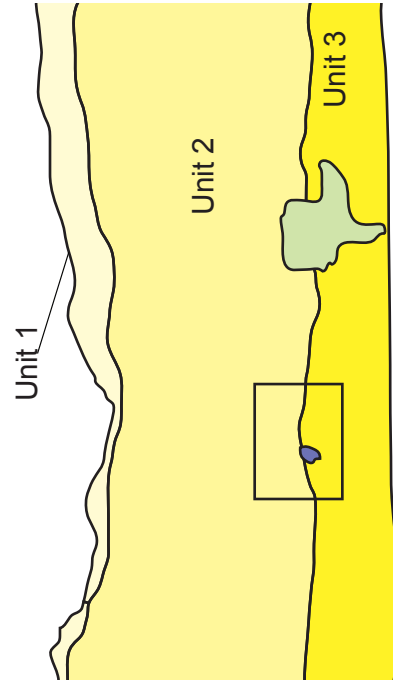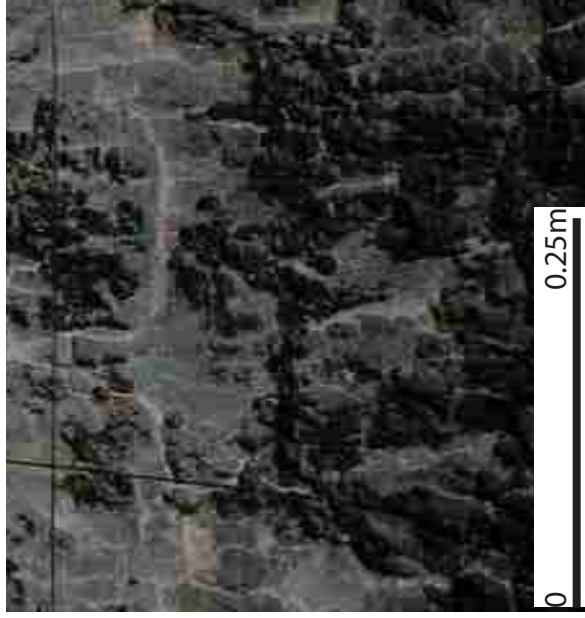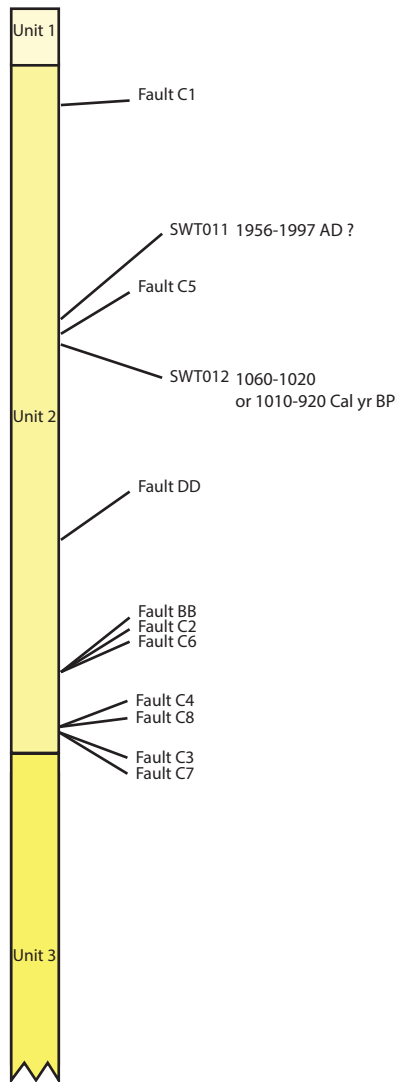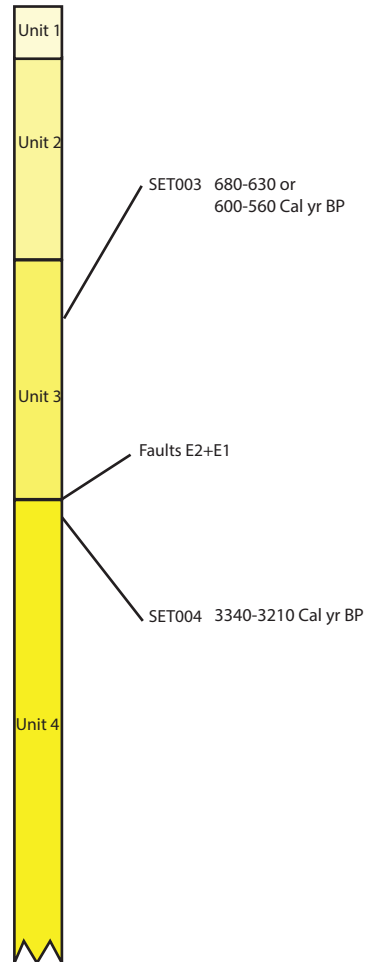
Figure 15. Photos of trench showing Krotovina (left) and Liquefaction (right). Krotovina and liquefaction marked with green nails. Unit 2 and 3 horizon marked by orange nails. Trench log beneath. Krotovina in blue. Liquefaction in grey.

Southwest Trench   Southeast Trench   North Trench

Southwest Trench

Unit 1

Fault C1

SWT011 1956-1997 AD ?

Fault C5

SWT012 1060-1020
or 1010-920 Cal yr BP

Unit 2

Fault DD

Fault BB
Fault C2
Fault C6

Fault C4
Fault C8

Fault C3
Fault C7

Unit 3

Southeast Trench

Unit 1

Unit 2

SET003   680-630 or
600-560 Cal yr BP

Unit 3

Faults E2+E1

SET004   3340-3210 Cal yr BP

Unit 4

North Trench

Unit 1

Unit 2

Unit 3

NET009   8640-8550
Cal yr BP ?

Fault $J2_2$
Fault $J4_2$

Fault GG

Fault $J2_1$

Fault HH

Brecciation FF
Brecciation KK
Brecciation LL
Fault J1

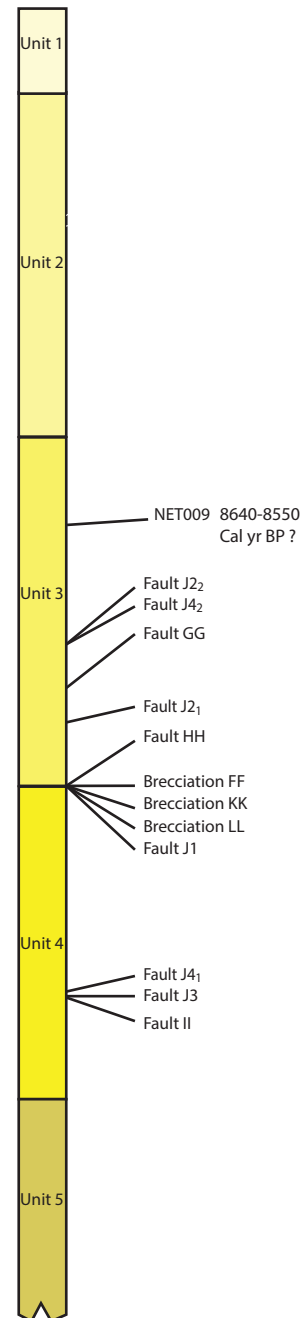Unit 4

Fault $J4_1$
Fault J3

Fault II

Unit 5

Figure 16. Locations of trench log features in relation to the defined trench units. Carbon date samples site with determined ages listed. Question marks indicate possible contaminated samples. Faults are located at the fault tip in relation to the host unit. When listed with subscript number, faults are interpreted to be reactivated, placement determined from differential unit offset. No historical records indicate an earthquake event on the SFS.
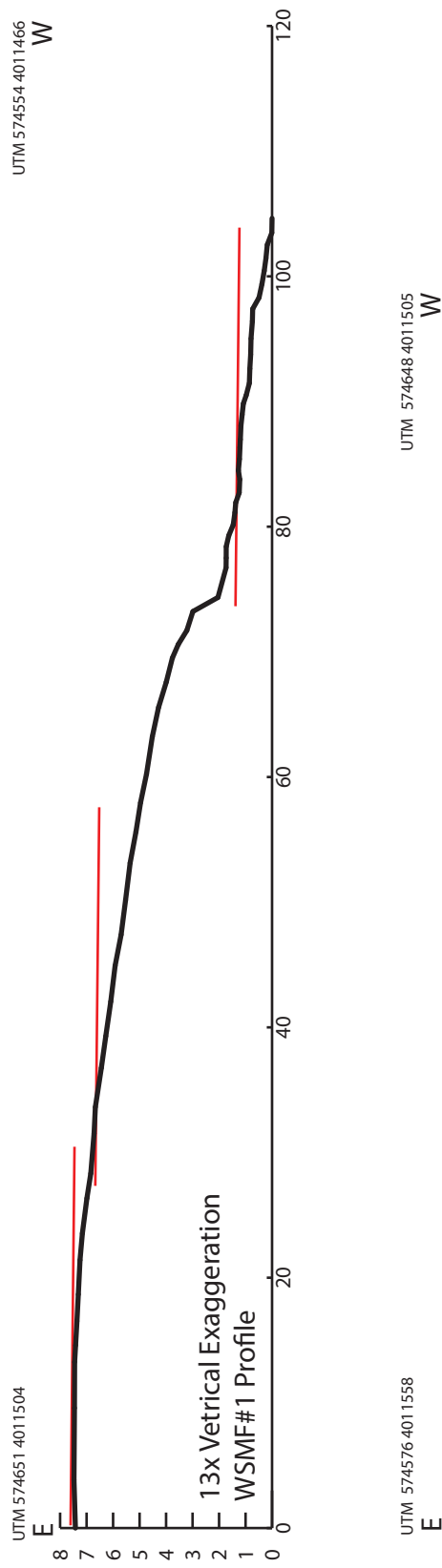
Figure 17. Topographic profiles of the West Spring Mountains. The profiles are taken crossing the WSMF fault scarp near Wheeler Pass road entering into Pahrump Valley. The red lines highlight the slope gradient with breaks caused by the occurrence of multiple scarp forming events.
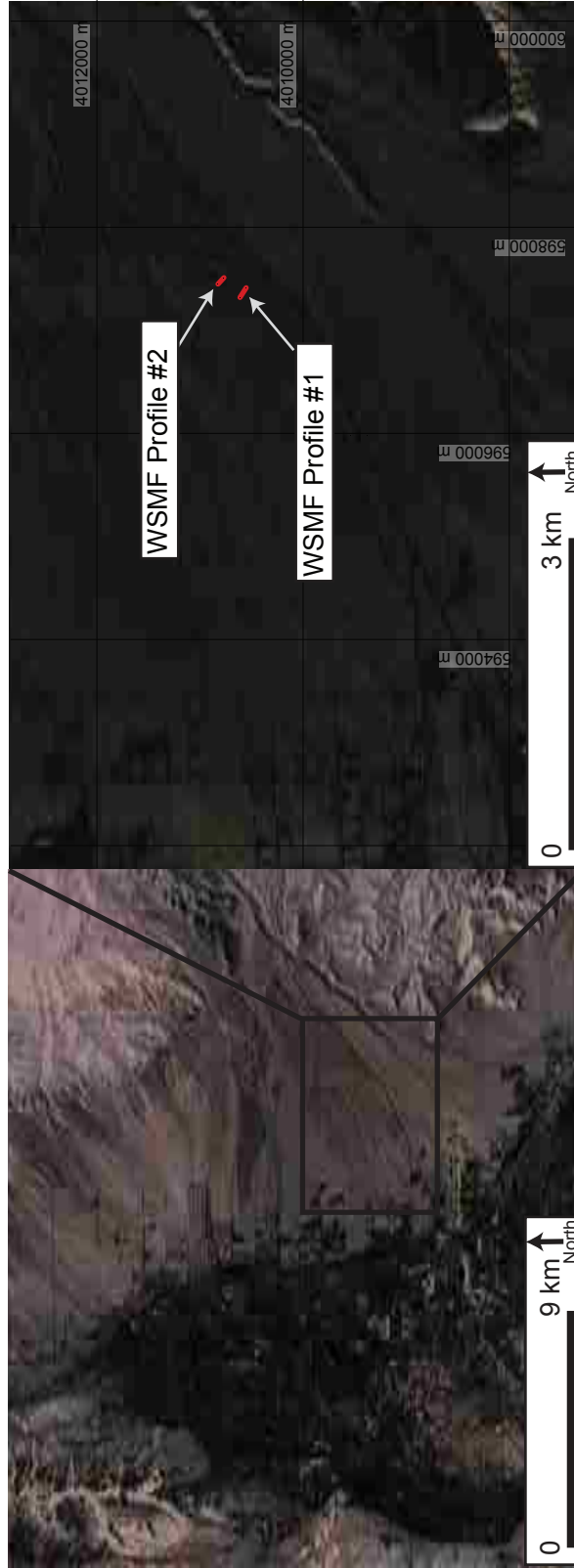
69

Figure 18. West Spring Mountain fault scarp locations the WSMF scarp were surveyed using a TOPCON Robotic Total Station to build topogrphic profiles for analysis. Transect locations are marked in red lines UTM grid shown. Profiles are shown on Figure 13.
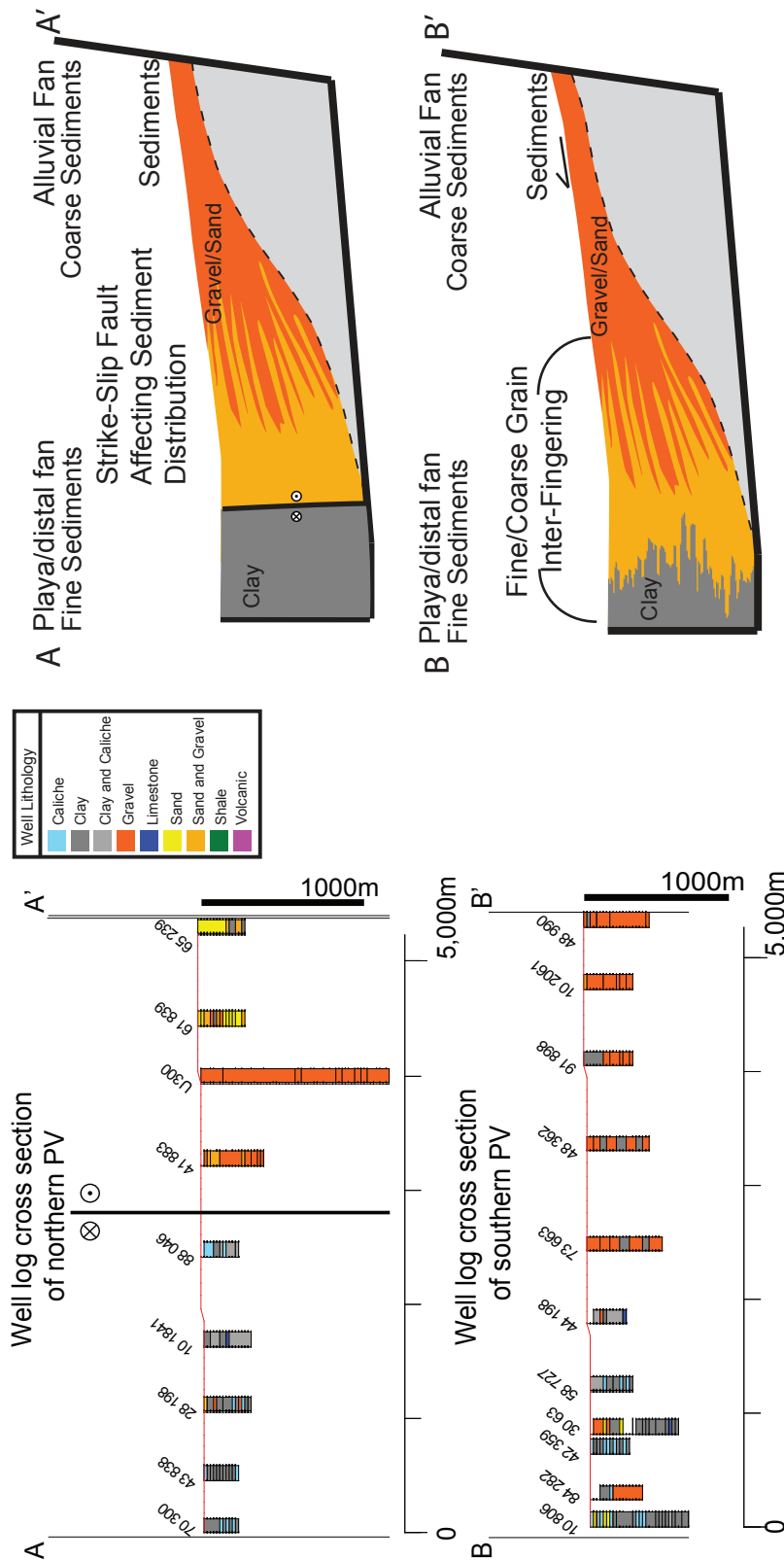
Figure 19. Pahrump well log cross sections. Top Left Figure: Well log based cross sections from the transects in Figure 15. The cross sections display the abrupt change in sediment grain size due to the tectonic transport of fine grained sediments. Cross section A-A' shows the fault surface with adjacent very fine grained sediments and coarse grained alluvial sediments. No interfingering is seen in the well logs across the fault surface indicating a lack of progradational/degradational alluvial/pluvial sediment deposition. Well log based cross section B-B' shows a nearby unfaulted interface between the fine and coarse grained sediments with interfingering of the units in the well log due to the progradational/degredational alluvial/pluvial sediment deposition.

APPENDIX 1 RADIOCARBON SAMPLE DATA

Six samples were collected from Stewart Valley in the trenches for radiocarbon analysis. The samples were examined by specialists at PaleoResearch Institute to estimate the age of deposition of the sediment horizons from which that the samples were collected. The samples were sifted to locate large organic particles appropriate for dating and then treated to extract microscopic charcoal and organic particles (Puseman and Scott Cummings, 2010). AMS radiocarbon dating was used on the samples to constrain the ages of sediment deposition with an ultimate goal of constraining the ages of fault surfaces, that cut or do not cut the sediment horizons (Puseman and Scott Cummings, 2010). Six AMS radiocarbon dates were obtained by the Paleoresearch Institute with: one date from microscopic charcoal, four dates from particulate soil organics, and one date achieved from the processing of soil humates (Puseman and Scott Cummings, 2010). Sample SET004 did not yield a sufficient amount of material for dating using the described methods. This sample was treated to date humates instead (Puseman and Scott Cummings, 2010).

The description of and material s extracted from the samples by Paleoresearch Institute are described in Tables 1, 2 and 3 (Puseman and Scott Cummings, 2010). The AMS analysis presents dates for each sample that are displayed in Tables 3 and 4 and Figures 20, 21, 22, 23, 24, 25 and 26 (Puseman and Scott Cummings, 2010).

TABLE 1
PROVENIENCE DATA FOR SAMPLES FROM TRENCHES AT PAHRUMP, NEVADA

Sample No	Trench	Context	Provenience/ Description	Analysis
011	SWT	Youngest uncut	Alluvium/playa sediments, estimated age of 6,000-12,000 years	Macrofloral Particulate soil organic extraction AMS ^{14}C Date
012		Oldest cut	Alluvium/playa sediments, estimated age of 6,000-12,000 years	Macrofloral AMS ^{14}C Date
003	SET	Youngest uncut	Alluvium/playa sediments, estimated age of 6,000-12,000 years	Macrofloral Particulate soil organic extraction AMS ^{14}C Date
004		Oldest cut	Alluvium/playa sediments, estimated age of 6,000-12,000	Macrofloral Humate AMS ^{14}C Date
009	NET	Youngest uncut	Alluvium/playa sediments, estimated age of 6,000-12,000	Macrofloral Particulate soil organic extraction AMS ^{14}C Date
010		Oldest cut	Alluvium/playa sediments, estimated age of 6,000-12,000 years	Macrofloral Particulate soil organic extraction AMS ^{14}C Date

TABLE 2
MACROFLORAL REMAINS FROM TRENCHES AT PAHRUMP, NEVADA

Sample No.	Identification	Part	Charred		Uncharred		Weights/ Comments
			W	F	W	F	
BWT011	Volume Water-Screened						1.0 quart
	Water-screened Sample Weight						13.460 g
	FLORAL REMAINS:						
	Rootlets					X	Few
	CHARCOAL/WOOD:						
	Conifer and Unidentified hardwood	Charcoal		X			< 0.0001 g
	NON-FLORAL REMAINS:						
	Bone					1	0.0044 g
	Insect	Chitin				1	
	Rock/Gravel					X	Few
BWT012	Volume Water-Screened						1.0 quart
	Water-screened Sample Weight						11.441 g
	FLORAL REMAINS:						
	Rootlets					X	Few
	CHARCOAL/WOOD:						
	Undiagnostic central pith and Unidentifiable - small**	Charcoal		X			0.0009 g
	NON-FLORAL REMAINS:						
	Insect					4	
	Rock/Gravel					X	Few
BET003	Volume Water-Screened						1.5 quart
	Water-screened Sample Weight						14.011 g
	FLORAL REMAINS:						
	Lepidium-type	Silique			11		
	Lepidium-type	Seed			1		
	Scrophulariaceae	Seed			1		
	Root	Bark				X	Few
	Rootlets					X	Few
	CHARCOAL/WOOD:						
	Chenopodiaceae-type	Wood				1	0.003 g

74

TABLE 2 (Continued)

Sample No.	Identification	Part	Charred W	Charred F	Uncharred W	Uncharred F	Weights/ Comments
BET003	NON-FLORAL REMAINS						
	Insect	Chitin				4	
	Rock/Gravel					x	Few
BET004	Volume Floated						1.0 quart
	Light Fraction Weight						0.242 g
	FLORAL REMAINS						
	Roots					x	Few
	Rootlets					x	Few
	NON-FLORAL REMAINS						
	Insect	Chitin				16	
	Insect fecal pellet					4	
	Gravel					x	Few
NET009	Volume Floated						1.0 quart
	Light Fraction Weight						0.475 g
	FLORAL REMAINS						
	Roots					x	Few
	Rootlets					x	Few
	CHARCOAL/WOOD						
	Unidentifiable - small** (combined with particulate soil organics to obtain date)	Charcoal		4			0.0004 g
	NON-FLORAL REMAINS						
	Rock/Gravel					x	Few
NET010	Volume Floated						1.0 quart
	Light Fraction Weight						0.432 g
	FLORAL REMAINS						
	Roots					x	Few
	Rootlets					x	Few
	CHARCOAL/WOOD						
	Unidentified hardwood - small	Charcoal		1			0.0001 g

TABLE 2 (Continued)

| Sample No. | Identification | Part | Charred | | Uncharred | | Weights/ |
			W	F	W	F	Comments
NET010	NON-FLORAL REMAINS						
	Bone					1	0.1123 g
	Insect	Chitin				5	
	Rock/Gravel					X	Few

W = Whole   F = Fragment

X = Presence noted in sample   g = grams

** = Submitted for AMS radiocarbon dating   mm = milimeters

76

TABLE 3
INDEX OF MACROFLORAL REMAINS RECOVERED FROM TRENCHES AT PAHRUMP, NEVADA

Scientific Name	Common Name
FLORAL REMAINS:	
Lepidium	Peppergrass
Scrophulariaceae	Figwort family
CHARCOAL/WOOD:	
Chenopodiaceae-type	similar to woody members of the Goosefoot family
Conifer	Cone-bearing, gymnospermous trees and shrubs, mostly evergreens, including the pine, spruce, fir, juniper, cedar, yew, hemlock, redwood, and cypress
Unidentified hardwood - small	Wood from a broad-leaved flowering tree or shrub, fragments too small for further identification
Undiagnostic central pith	Central pith; consists of parenchyma with no diagnostic elements

TABLE 4
RADIOCARBON RESULTS FOR SAMPLES FROM PAHRUMP, NEVADA

Sample No.	Sample Identification	AMS ¹⁴C Date*	1-sigma Calibrated Date (68.2%)	2-sigma Calibrated Date (95.4%)	δ¹³C** (‰)
PRJ-10-100-SWT011	Particulate soil organics	1.0968 fM	June-October 1957; February-April 1996; March-July 1997	December 1956-November 1957; April 1995; January-May 1996; August 1996; January-July 1997	-21.7
PRJ-10-100-SWT012	Unidentified charcoal	1075 ± 20 RCYBP	1050-1030; 990-930 CAL yr. BP	1060-1020; 1010-930 CAL yr. BP	-13.9
PRJ-10-100-SET003	Particulate soil organics	685 ± 25 RCYBP	670-640; 590-560 CAL yr. BP	680-630; 600-560 CAL yr. BP	-15.2
PRJ-10-100-SET004	Humates (Soil organic compounds)	3045 ± 15 RCYBP	3330-3280; 3270-3240; 3230-3220 Cal yr. BP	3340-3210 CAL yr. BP	-9.0
PRJ-10-100-NET009	Unidentifiable charcoal and Particulate soil organics	7820 ± 30 RCYBP	8650-8500; 8570-8560 CAL yr. BP	8640-8550 CAL yr. BP	-15.1
PRJ-10-100-NET010	Particulate soil organics	1.0328 fM	July 1955-August 1956	August 1954-December 1956	-13.9

* Reported in radiocarbon years at 1 standard deviation measurement precision (68.2%), corrected for δ¹³C.

** δ¹³C values are measured by AMS during the ¹⁴C measurement. The AMS-δ¹³C values are used for the ¹⁴C calculation and should not be used for dietary or paleoenvironmental interpretations.

fM = fraction Modern. Recent dates (falling within the time after atomic testing began) are reported as fraction Modern because calibrations can only be done using fraction Modern for this time period. Years BP are calculated as prior to 1950, not today's date.

Figure 20. PRI Radiocarbon Age Calibration SWT012

Laboratory Number: PRI-10-100-SWT011
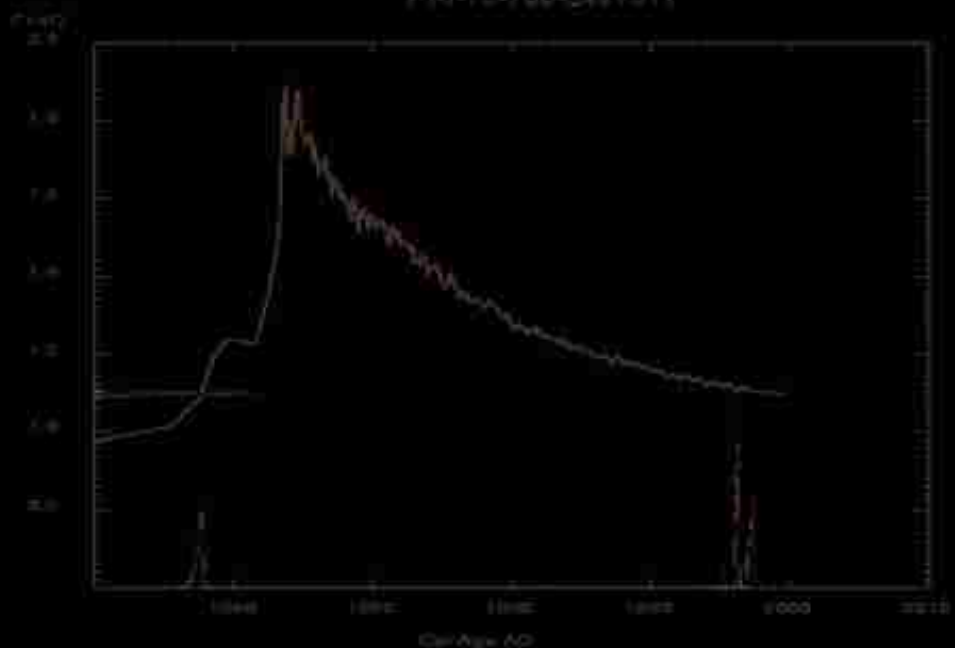Sample Identification: Particulate soil organics
Conventional AMS ¹⁴C Date: 1.0168 ± 0.0027 fM
1-sigma Calibrated Age Range (68.2%): (32.61%) June-October 1957; (33.06%) February-April 1995; (35.52%) March-July 1997
2-sigma Calibrated Age Range (95.4%): (19.97%) December 1955-November 1957; (0.50%) April 1985; (27.16%) January-May 1995; (6.30%) August 1995; (21.44%) January-July 1997
δ¹³C (‰): -21.7 (Measured for ¹⁴C calculation, not valid for dietary or paleoenvironmental interpretations)

PRI-10-100-SWT011

Cal Age AD

Intercept Statement. PRI utilizes CALIB 6.1.0 (Stuiver, Reimer 2005) for radiocarbon calibration, which is a probability-based method for determining conventional ages. This method is preferred over the intercept-based alternative because it provides a calibrated date that reflects the probability of its occurrence within a given distribution (reflected by the amplitude (height) of the curve), as opposed to individual point estimates. As a result, the probability-based method offers more stability to the calibrated values than those derived from intercept-based methods that are subject to adjustments in the calibration curve (Telford 2004).

Laboratory Number: PRI-10-100-SET004
Sample Identification: Humates (soil organic compounds)
Conventional AMS ¹⁴C Date: 3045 ± 15 RCYBP
1-sigma Calibrated Age Range (68.2%): 3330-3260; 3270-3240; 3230-3220 Cal. yr. BP
2-sigma Calibrated Age Range (95.4%): 3340-3210 Cal. yr. BP
δ¹³C [‰]: -9.0 (Measured for ¹⁴C calculation, not valid for dietary or paleoenvironmental interpretations)

Figure 22. PRI Radiocarbon Age Calibration SET004

Laboratory Number: PRI-10-100-SET003
Sample Identification: Particulate soil organics
Conventional AMS ^{14}C Date: 665 ± 25 RCYBP
1-sigma Calibrated Age Range (68.2%): 670-640; 580-560 CAL yr BP
2-sigma Calibrated Age Range (95.4%): 680-630; 600-560 CAL yr BP
δ^{13}C (‰): -15.2 (Measured for ^{14}C calibration, not valid for dietary or paleoenvironmental reinterpretations)
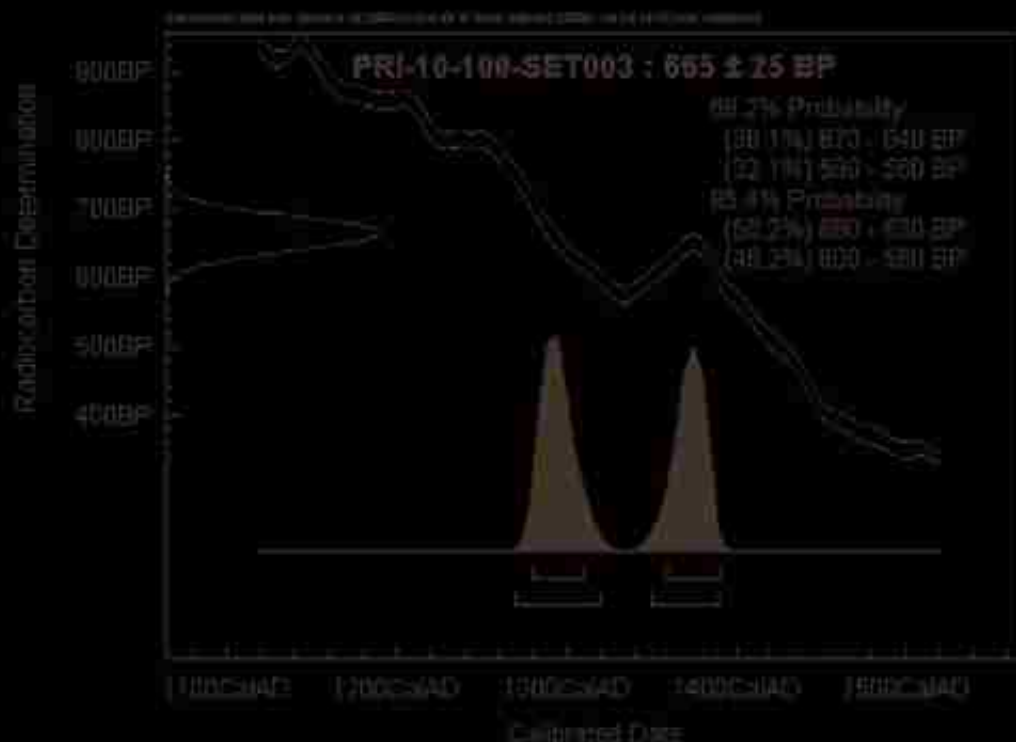
Intercept Statement: PRI utilizes OxCal 3.10 (Bronk Ramsey 2005) for radiocarbon calibration, which is a probability-based method for determining conventional ages. This method is preferred over the intercept-based alternative because it provides a calibrated date that reflects the probability of its occurrence within a given distribution (reflected by the amplitude (height) of the curve), as opposed to individual point estimates. As a result, the probability-based method offers more stability to the calibrated values than those derived from intercept-based methods that are subject to adjustments in the calibration curve (Telford 2004).

Figure 23. PRI Radiocarbon Age Calibration SET003

Laboratory Number: PRI-10-100-NET010
Sample Identification: Particulate soil organics
Conventional AMS ^{14}C Date: 1.0225 ± 0.0025 fM
1 sigma Calibrated Age Range (68.2%): (100%) mar 1965 - August 1966
2 sigma Calibrated Age Range (95.4%): (100%) August 1964 - December 1966
δ^{13}C (‰): -13.8 (Measured for ^{14}C calculation, not valid for dietary or paleoenvironmental interpretations)

PRI-10-100-NET010

Intercept Statement: PRI utilizes OxCal2 10 (Bronk Ramsey 2005) for radiocarbon calibration, which is a probability-based method for determining conventional ages. This method is preferred over the intercept-based alternative because it provides a calibrated date that reflects the probability of its occurrence within a given distribution (reflected by the amplitude (height) of the curve), as opposed to individual point estimates. As a result, the probability-based method offers more stability to the calibrated values than those derived from intercept-based methods that are subject to adjustments in the calibration curve (Telford 2004).

Figure 24. PRI Radiocarbon Age Calibration NET010
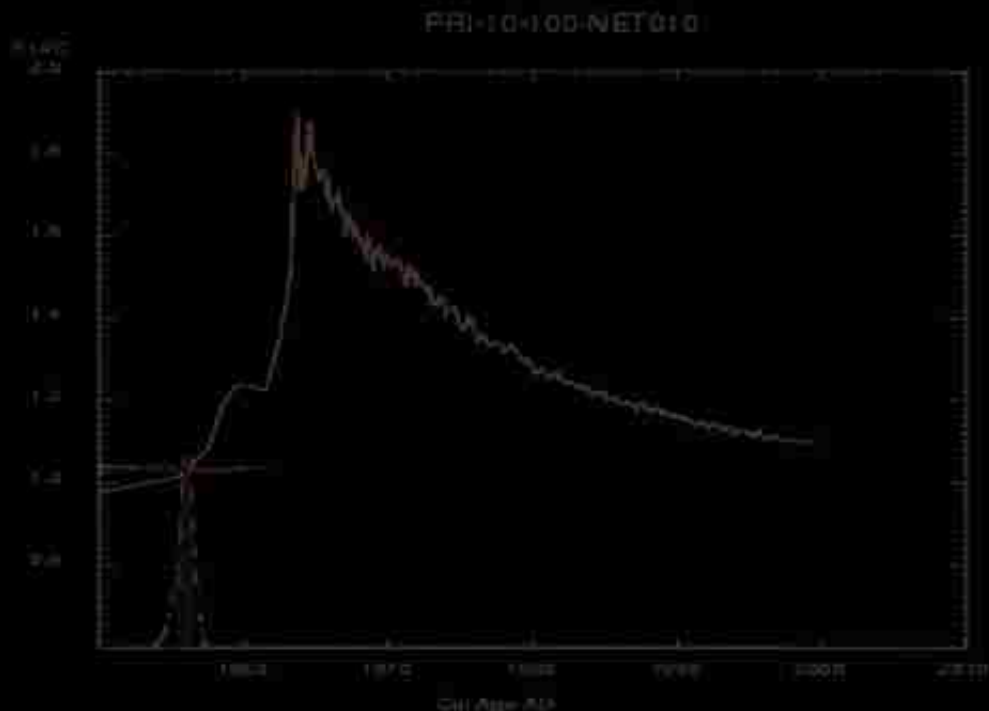
Laboratory Number: PRI-10-100-NWT009
Sample Identification: Particulate soil organics + unidentifiable charcoal
Conventional AMS ¹⁴C Date: 7820 ± 20 RCYBP
1-sigma Calibrated Age Range (68.2%): 8630–8580; 8570–8550 CAL yr. BP
2-sigma Calibrated Age Range (95.4%): 8640–8550 CAL yr. BP
δ¹³C (‰) = -15.1 (Measured for ¹⁴C calculation, not valid for dietary or paleoenvironmental interpretations)

PRI-10-100-NWT009 : 7820 ± 20 BP

68.2% Probability
(60.1%) 8630-8580 BP
(8.1%) 8570-8560 BP
95.4% Probability
(95.4%) 8640-8550 BP

Intercept Statement: PRI utilizes OxCal3.10 [Bronk Ramsey 2005] for radiocarbon calibration, which is a probability-based method for determining commensurate ages. This method is preferred over the intercept-based alternative because it provides a calibrated date that reflects the probability of its occurrence within a given distribution (reflected by the amplitude (height) of the curve), as opposed to individual point estimates. As a result, the probability-based method offers more stability to the calibrated values than those derived from intercept-based methods that are subject to adjustments in the calibration curve (Telford 2004).

Figure 25. PRI Radiocarbon Age Calibration NWT009

APPENDIX 2 WELL LOG DATABASE

See attached DVD Excel file <u>PahrumpWelllogs.xls</u>

APPENDIX 3 STEWART VALLEY CORE LOG

Stewart Valley Test Well   **Location: 0575745, 4010075 UTM**

Drilled by Eagle Drilling

Lithology	**Depth (Top)**		**Comments**
	Feet	Meters	
Reddish Brown Clay	10	3.8	Top 1/3 has 1 mm - 1 cm white calcite nodules. Bio #1 is 12" from top
Reddish Tan Clay	14	5.32	Contains 1-2 mm white calcite nodules. Bio #2 is 13" from the top
Gray Tan Clay	16	6.08	Contains 1-2 mm white calcite nodules.
Grayish Brown Clay	17	6.46	Contains lenses and nodules of white and red/brown clay
Reddish Tan Clay	20	7.6	Contains small nodules of white clay, some rare nodules of green and yellow clay. Bio #4 is 14" from top, bio #5 is 4" from top
Red Tan Clay	22	8.36	Has rounded dark clast 1.3 cm in diameter.

Greyish White Clay	26	9.88	Has a green tint near the top. Some 1-2 mm diameter (gypsum?) nodules half way down and increasing toward the bottom. Bio #6 is 16" from top, Bio #7 is 31" from top
White Tan Clay	30	11.4	Red clay lenses and 1-2 mm nodules of gypsum. Retains water and contains Bio #8 14" from top
White Tan Clay	32	12.16	Contains 1-2 mm gypsum nodules near bottom.
White Green Tan Clay	33	12.54	Water holding clay.
Greenish Gray Clay	34	12.92	Contains white clay lenses. Contains Bio #10
Green Clay	35	13.3	Turns light greenish tan at the bottom, lenses of white clay at the top.
White Tan Clay	40	15.2	Holds a lot of water and contains green clay lenses.
Tan Clay	42	15.96	Contains white clay lenses and contains Bio #11 and Bio #12
Reddish Tan Clay	43	16.34	Contains lots of (gypsum?) nodules.

			Gets darker tan downward and contains Bio #14
Light Brown Clay	47	17.86	White clay nodules 1-2 mm and lenses of white clay.
Light Red Brown Clay	50	19	White clay lenses and white clay nodules 1-2mm
Tan Clay	53	20.14	Lenses of red tan clay anf contains Bio #15
Light Tan Clay	55.5	21.09	Gets slightly darker near bottom and it has a yellowish tint.
Tan Clay	60	22.8	Homogeneous
Pale Red Brown Clay	66	25.08	Gradational contact
Gray Clay	67.5	25.65	Turns green downward
Light Tan Clay	70	26.6	Contains white gypsum nodules
Light Brown Clay	90	34.2	Homogeneous
Light Brown Clay	110	41.8	Contains grey clay nodules that are a few mm thick.
Light Brown Clay	120	45.6	Contains green and reddish clay nodules that are several mm thick and white calcite nodules up to 1 mm thick.

Brown Clay	140	53.2	Green and reddish clay nodules that are several mm thick, calcite nodules that are a few mm thick.
Light Brown Clay	150	57	Contains Reddish brown, green, and white clay nodules several mm thick and white calcite nodules a few mm thick .
Light Tan/Grayish Clay	170	64.6	Contains green and white clay nodules that are several mm thick and white calcite nodules 1-2 mm thick.
Light Tan Clay	180	68.4	Contains red clay several mm thick and white calcite nodules a couple mm thick.
Light Brown Clay	190	72.2	Contains red and white clay nodules that are several mm thick and white calcite nodules 1-2 mm thick.
Light Brown Clay	200	76	Contains white clay nodules several mm thick and white calcite nodules a few mm thick.
Tan Clay	230	87.4	reddish and green clay nodules that are several mm thick.

Light Brown Clay	240	91.2	Contains white and brown clay nodules several mm thick.

Bio# (1-15) are biological samples collected to be analyzed

APPENDIX 4 TRENCH LOG

See attached DVD File Plate 1.pdf

BIBLIOGRAPHY

Ambraseys, N. N., 1988, Engineering Seismology: earthquake engineering and
structural dynamics: Journal of the International Association of Earthquake
Engineering, v. 17, p. 1-105.

Anderson, R. E., compiler, 1999, Fault number 1117, Frenchman Mountain fault,
in Quaternary fault and fold database of the United States: U.S. Geological
Survey website, http://earthquakes.usgs.gov/regional/qfaults, accessed
04/07/2012.

Anderson, R. E., Bucknam, R. C., Crone, A. J., Haller, K. M., Machette, M. N.,
Personius, S. F., Barnhard, T. P., Cecil, M. J., and Dart, R. L., 1995,
Characterization of Quaternary and suspected Quaternary faults, regional
studies, Nevada and California: U.S. Geological Survey Open-File Report
95-599, 70 pp.

Bronk, R. C., 2005, OxCal. 3.1 ed. www.rlaha.ox.ac.uk/oxcal/oxcal.htm.

Telford, R. J., Heegaard, E., Birks, H. J., 2004, The Intercept is a Poor Estimate
of a Calibrated Radiocarbon Age. The Holocene, v 14, p. 296-298.

Andrew J. E.and Walker J. D., 2012, Reconstructing late Cenozoic deformation
in central Panamint Valley, California: Evolution of slip partitioning in the
Walker Lane: Geosphere, v. 5, p.172-198. doi: 10.1130/GES00178.1

Bacon, S.N. and Pezzopane, S.K., 2007, A 25,000-year record of earthquakes
on the Owens Valley fault near Lone Pine, California: Implications for
recurrence intervals slip rates, and segmentation models: Geological
Society of America Bulletin, v. 119, p. 823–847.

Bacon, S.N., Pezzopane, S.K., and Burke, R.M., 2002, Paleoseismology on the Owens Valley fault and Holocene stratigraphy of pluvial Owens Lake near Lone Pine, eastern California: Geological Society of America Abstracts programs, v. 34, p. 27.

Beanland, S., and Clark, M. M., 1994, The Owens Valley fault zone, eastern California and surface rupture associated with the 1872 earthquake: U.S. Geological Survey Bulletin 1982, 29 pp.

Bennett, R. A., Davis, J. L., and Wernicke, B. P., 1998, Present-day pattern of Cordilleran deformation in the western United States: Geology, v. 27, p. 371-374.

Bennett, R. A., Wernicke, B. P., and Davis, J. L., 1998, Continuous GPS measurements of contemporary deformation across the northern Basin and Range province: Geophysical Research Letters, v. 25, p. 563-566.

Bennett, R. A., Wernicke, B. P., Niemi, N. A., Friederich, A. M., and Davis, J. L., 2003, Contemporary strain rates in the northern Basin and Range province from GPS data: Tectonics, v. 22, p. 1008-1010.

Birkeland, P., 1999, Soils and geomorphology: New York, Oxford University Press, 430 p.

Billingsley, P., and Locke, A., 1941, Structure of ore districts in the continental framework: Transactions of the American Institute of Mining and Metallurgical Engineers, v. 144, p. 9-59.

Bucknam, R. C., and Anderson, R. E., 1979. Estimation of fault-scarp ages from a scarp height-slope-angle relationship: Geology, v. 7, p.11-14.

Burchfiel, B.C., Hamill, G.S., and Wilhelms, D.E., 1983, Structural geology of the Montgomery Mountains and the northern half of the Nopha and Resting Spring Ranges, Nevada and California: Geological Society of America Bulletin, v. 94, p. 1359.

Carr, W. J., 1984, Regional structural setting of Yucca Mountain, southwestern Nevada, and Late Cenozoic rates of tectonic activity in part of the southwestern Great Basin, Nevada and California: U.S. Geological Survey Open File Report 84-854, 109 pp.

Carr, W. J., 1988, Geology of the Devils Hole area, Nevada: U.S. Geological Survey Open-File Report 87-560, 34 pp.1116.

Carter, J., Taylor, W., and Luke, B,. 2008. Structural and sedimentological development of Pahrump basin, southern Nevada with implications for seismic hazards: EOS Trans. American Geophysical Union, v. 8, n. 53, Fall Meeting, Abstract T21B-1970.

DeMets, C., and Dixon, T. H., 1999, New kinematic models for Pacific-North America motion from 3 Ma to present, I: Evidence for steady motion and biases in the NUVEL-1A model; Geophysical Research Letters., v. 26, p. 1921-1924.

DeMets, C., Gordon, R. G., Stein, S., and Argus, D. F., 1987, A revised estimate of Pacific-North America motion and implications for western North America plate boundary zone; Geophysical Research Letters, v. 14, p. 911-914.

dePolo, C. M., 1998, A reconnaissance technique for estimating the slip rates of normal-slip faults in the Great Basin, and application to faults in Nevada,

U.S.A [Ph.D. thesis]: United States (USA), University of Nevada at Reno, Reno, NV, United States (USA), 199 pp.

dePolo, C. M., Ramelli, A. R., and Bell, J. W., 2003, Preliminary geologic map of the Sixmile Spring quadrangle, Nye county, Nevada, and Inyo County, California: Nevada Bureau of Mines and Geology Open-File Report 03-11 Map 1:24000, 1 sheet.

dePolo, C. M., Bell, J.W., Boron, S., Slemmons, D.B., and Werle, J.L., 2006, Latest Quaternary Fault Movement along the Las Vegas Valley Fault System, Clark County, Nevada: Environmental & Engineering Geoscience, v. 12, p. 181-193.

Dixon, T. H., Robaudo, S., Lee, J., and Reheis, M. C., 1995, Constraints on present-day Basin and Range deformation from space geodesy: Tectonics, v. 14, p. 755-772.

Dokka, R. K., 1983, Displacements on late Cenozoic strike-slip faults of the central Mojave Desert, California: Geology, v. 11, p. 305-308.

Dokka, R. K., and Travis, C. J., 1990, Late Cenozoic strike-slip faulting in the Mojave Desert, California: Tectonics, v. 9, p. 311-340.

Donovan, D. E., 1991, Neotectonics of the southern Amargosa Desert, Nye County, Nevada and Inyo County, California: University of Nevada, Reno M.S. thesis 2755, 151 pp.

Doser, D., and Smith, R., 1989, An assessment of source parameters of earthquakes in the Cordillera of Western United States: Bulletin of the Seismological Society of America, v. 79, p. 1383-1409.

Ferguson, H. G., and Muller, S. W., 1949, Structural geology of the Hawthorne and Tonopah quadrangles, Nevada: U.S. Geological Survey Professional Paper 216, 55 pp.

Fleck, R.J., 1971, Tectonic style, magnitude, and age of deformation in the Sevier orogenic belt in southern Nevada and eastern California; reply: Geological Society of America Bulletin, v. 82, p. 1437-1440.

Frankel, F., Glazner, A., Kirby, E., Monastero, F., Strane, M., Oskin, M., Unruh, J., Walker, J., Anadakrishnan, S., Bartley, J., Coleman, D., Dolan, J., and Finkel, R., 2008, Active tectonics of the eastern California shear zone: Geological Society of America Field Guide 11, p. 43-84.

Frankel, K. L., Dolan, J. F., Owen, L. A., Ganev, P., Finkel, R. C., 2011, Spatial and temporal constancy of seismic strain release along an evolving segment of the Pacific–North America plate boundary: Earth and Planetary Science Letters, v. 304, p. 565–576.

Gan, W., Svarc, J. L., Savage, J. C., and Prescott, W.H., 2000, Strain accumulation across the eastern California shear zone at latitude 36°30'N: Journal of Geophysical Research, v. 105, p. 16229- 16236.

Gianella, V. P. and Callaghan, E., 1934, The earthquake of December 20, 1932, at Cedar Mountain, Nevada and its bearing on the genesis of Basin and Range structure: Journal of Geology, v. 47, p. 1-22.

Guest, B., Niemi, N., and Wernicke, B., 2007, Stateline fault system; a new component of the Miocene-Quaternary Eastern California shear zone: Geological Society of America Bulletin, v. 119, p. 1337-1346.

Hanks, T. C. and Boore, D. M., 1984, Moment-magnitude relations in theory and practice: Journal of Geophysical Research, p. 6229-6236.

Hearn, E. H. and Humphreys, E. D., 1998, Kinematics of the southern Walker Lane Belt and motion of the Sierra Nevada block, California: Journal of Geophysical Research, v. 103, p. 27,033–27,049.

Hewett, D. F., 1956, Geology and mineral resources of the Ivanpah Quadrangle, California and Nevada: U. S. Geological Survey, Reston, VA, United States (USA), Report P 0275, 172 pp.

Hoffard, J. L., 1991, Quaternary tectonics and basin history of Pahrump and Stewart Valley, Nevada and California [M.S. Thesis]: Reno, University of Nevada, 138 pp.

Hislop, A., 2012 Bedrock Expression of the Eastern California Shear Zone: southern Stateline Fault California/ Nevada [M.S. Thesis]:University of Calgary, 109 pp.

Ishihara, K., 1985, Stability of natural deposits during earthquakes: Proceedings of the 11th International Conference on Soil Mechanics and Foundation Engineering, San Francisco, v. 1, p. 321-376.

Klinger, R. E., and Piety, L. A., 2000, Late Quaternary tectonic activity on the Death Valley and Furnace Creek faults, Death Valley, California, in Geologic and Geophysical Characterization Studies of Yucca Mountain, Nevada, A Potential High-Level Radioactive-Waste Repository: United States Geological Survey, ch. H, p. 1 –16.

Lee, J., Spencer, J., and Owen, L., 2001, Holocene slip rates along the Owens Valley fault, California: Implications for the recent evolution of the Eastern California shear zone: Geology, v. 29, p. 819-822.

Liggett, M. A., and Childs, J. F., 1978, Evidence of a major fault zone along the California-Nevada state line, 35°30'N to 36°30'N latitude: NASA technical reports, CR-133140, E73-10773, p. 1-13.

Locke, A., Billingsley, P. R., and Mayo, E. B., 1940, Sierra Nevada tectonic patterns: Geological Society of America Bulletin, v. 51, p. 513-539.

Louie, J., Shields, G., Ichinose, G., Hasting, M., Plank, G., and Bowman, S., 1998, Shallow geophysical constraints on displacement and segmentation of the Pahrump Valley fault zone; Seismic hazards in the Las Vegas region: Nevada Bureau of Mines and Geology, Reno, NV, United States (USA), Report 98-6, p. 79-85.

Malmberg, G.T., 1967. Hydrology of the valley-fill and carbonate rock reservoirs, Pahrump Valley, Nevada-California: U.S. Geological Survey, Water Supply Paper 1832, 47 pp.

Mason, D. B., 1996, Earthquake magnitude potential of the Intermountain Seismic Belt, USA, from surface-parameter scaling of late Quaternary faults: Bulletin of the Seismological Society of America, v. 86, p. 1487-1506.

McClusky, S., Bjornstad, S., Hager, B., King, R., Meade, B., Miller, M., Monastero, F., and Souter, B., 2001, Present day kinematics of the eastern California shear zone from a geodetically constrained block model: Geophysical Research Letters, v. 28, p. 3369-3372.

Miall, A. D., 1990, Principles of sedimentary basin analysis, second edition: New York, Springer-Verlag, 668 pp.

Minster, J. B., and Jordan, T. H. , 1987, Vector constraints on western U.S. deformation from space geodesy, neotectonics, and plate motions: Journal of Geophysical Research, v. 92, p. 4798-4804.

National Research Council, 1985, Liquefaction of soils during earthquakes: National Academy Press, Washington, D.C., 240 pp.

Nielsen, R.L., 1965, Right-lateral strike-slip faulting in the Walker Lane, west-central Nevada: Geological Society of America Bulletin, v. 76, p. 1301-1308.

Oldow, J. S., Aiken, C. L. V., Hare, J. L., Ferguson, J. F., and Hardyman, R. F., 2001, Active displacement transfer and differential block motion within the central Walker Lane, western Great Basin: Geology, v. 29, p. 19–22.

Oldow, J. S., Kohler, G., Donelick R. A., 1994, Late Cenozoic extensional transfer in the Walker Lane strike-slip belt, Nevada: Geology, v. 22, p. 637–640.

Oldow, J. S., 1992, Late Cenozoic displacement partitioning in the northwestern Great Basin, in Craig, S. D., ed., Structure, tectonics, and mineralization of the Walker Lane, in Walker Lane Symposium Proceedings Volume: Reno, NV, Geological Society of Nevada, p.17–52.

Oldow, J. S., Bally, A. W., Ave Lallemant, H. G., and Leeman, W. P., 1989, Phanerozoic evolution of the North American Cordillera (United States and Canada), in Bally, A. W., and Palmer, A. R., eds., The geology of North

America: An overview: Boulder, CO, Geological Society of America, Geology of North America, Volume A, p. 139–232.

O'Leary, D. W., 2000,Tectonic significance of the Rock Valley fault zone, Nevada Test Site, in Whitney, J. and Keefer, W . R., eds., Geologic and geophysical characterization studies of Yucca Mountain, Nevada, a potential high-level radioactive waste repository: United States Geological Survey Digital Data Series v. 58, chapter 1,13 pp.

Oskin, M., Perg, L., Blumentritt, D., Mukhopadhyay, S., and Iriondo, A., 2007, Slip rate of the Calico fault: Implications for geologic versus geodetic rate discrepancy in the Eastern California Shear Zone: Journal of Geophysical Research, v. 112, p. 1-16, doi:10.1029/2006JB004451.

Oskin, M., and Iriondo, A., 2004, Large-magnitude transient strain accumulation on the Blackwater Fault, Eastern California shear zone: Geology, v. 32, p. 313-316.

Puseman, K, Scott Cummings, L, 2010, Examination of bulk sediment samples, microcharcoal extraction, and AMS radiocarbon analysis of alluvium from paleoseismic trenches at Pahrump, Nevada: PaleoResearch Institute Technical Report 10-100, 21 pp.

Peltzer, G., Crampe, F., Hensley, S., and Rosen, P., 2001, Transient strain accumulation and fault interaction in the eastern California shear zone: Geology, v. 29, p. 975-978.

Reheis, M. C., and Dixon, T. H. , 1996, Kinematics of the Eastern California
Shear Zone: Evidence for slip transfer from Owens and Saline Valley fault
zones to Fish Lake Valley fault zone: Geology, v. 24, p. 339–342.

Ryall, A., Slemmons, D. B., and Gedney, L D., 1966, Seismicity, tectonism, and
surface faulting in the western United States during historic time: Bulletin of
the Seismological Society of America, v. 56, p. 1105-1135.

Saldaña, S., 2009, Pseudo 3-D imagery of the state line fault system Stewart
Valley, Nevada using seismic reflection data [M.S. Thesis]: New Mexico
Institute of Mining and Technology, 54 pp.

Saldaña, S. C., Snelson, C. M., Taylor, W. J., and Zaragoza, S. A, 2006, Seismic
Investigation of Faulting in the River Mountains, Henderson, Nevada: Eos
Transactions, American Geophysical Union, v. 87, no. 52, Fall Meeting,
Abstract NS41A-1116.

Sauber, J., Thatcher, W., Solomon, S., and Lisowski, M., 1994, Geodetic slip rate
for the eastern California shear zone and the recurrence time of Mojave
Desert earthquakes: Nature, v. 367, p. 264-266.

Savage, J. C., Lisowski, M., and Prescott, W. H., 1990, An apparent shear zone
trending north-northwest across the Mojave Desert into Owens Valley,
eastern California: Geophysical Research Letters, v. 12, p. 2113–2116.

Scheirer, D.S., Sweetkind, D.S., and Miller, J.J., 2010, Multiple phases of basin
formation along the Stateline fault system in the Pahrump and Mesquite
Valleys, Nevada and California Geosphere: v. 6, p. 93-129,
doi:10.1130/GES00520.1

Schweickert, R. A., and Lahren, M. M., 1997, Strike-slip fault system in
Amargosa Valley and Yucca Mountain, Nevada: Tectonophysics, v. 272, p.
25-41.

Sieh, K. E., and Jahns, R. H., 1984, Holocene activity of the San Andreas Fault
at Wallace Creek, California: Geological Society of America Bulletin; v. 95,
p. 883-896.

Smith, R. B., and Sbar, M. L., 1974, Contemporary tectonics and seismicity of the
western United States with emphasis on the Intermountain Seismic Belt:
Geological Society of America Bulletin, v. 85, p. 1205-1218.

Smith, R. B., and Arabasz, W. J., 1991, Seismicity of the Intermountain seismic
belt, in Slemmons, D. B., et al., eds., Neotectonics of North America:
Boulder, Colorado, Geological Society of America, Decade Map Volume, p.
185–228.

Snow, J.K., and Wernicke, B.P., 2000, Cenozoic tectonism in the central Basin
and Range: Magnitude, rate and distribution of upper crustal strain:
American Journal of Science, v. 300, p. 659–719, doi: 0.2475/ajs.300.9.659.

Stewart, J. H., 1980, Geology of Nevada: Nevada Bureau of Mines and Geology
Special Publications, v. 4, p. 1-136.

Stewart, J. H., 1988, Tectonics of the Walker Lane Belt, western Great Basin;
Mesozoic and Cenozoic deformation in a zone of shear; Metamorphism and
crustal evolution of the Western United States: Rubey Volume VII:
Englewood Cliffs, New Jersey, Prentice-Hall, Volume, v. 7, Pretence Hall, p.
683-713.

Surpless, B., 2008, Modern strain localization in the central Walker Lane, Western United States; implications for the evolution of intraplate deformation in transtensional settings: Tectonophysics, v. 457, p. 239-253.

Thatcher, W., Foulger G. R., Julian B. R., Svarc J. L., Quilty E., and Bawden G. W., 1999, Present-day deformation across the Basin and Range province, western United States, Science, v. 283, p. 1714-1717.

U.S. Geological Survey and Nevada Bureau of Mines and Geology, 2006, Quaternary fault and fold database for the United States, accessed 2005, from USGS web site: http//earthquake.usgs.gov/regional/qfaults/.

Wallace, R. E., 1984, Patterns and timing of Late Quaternary faulting in the Great Basin Province and relation to some regional tectonic features: Journal of Geophysical Research, v. 89, p. 5763–5769.

Wells, D.L., and Coppersmith, K.J., 1994, New empirical relationships among magnitude, rupture length, rupture width, rupture area, and surface displacement: Bulletin of the Seismological Society of America, v. 84, p. 974-1002.

Wernicke, B. P. 1992, Cenozoic extensional tectonics of the U. S. Cordillera, in The Cordilleran Orogen: Conterminous U. S., B. C. Burchfiel, P. W. Lipman, and M. L. Zoback (Eds.); Geological Society of America, Boulder, Colorado, p. 553-581.

Wernicke, B., Davis, J. L., Bennett, R. A., Normandeau, J. E., Friedrich A. M., and Niemi, N. A., 2004, Tectonic implications of a dense continuous GPS

velocity field at Yucca Mountain, Nevada: Journal of Geophysical Research, v. 109, B12404, doi:10.1029/2003JB002832.

Wesnousky, S. G., 2005, Active faulting in the Walker Lane: Tectonics, v. 24, TC3009.

Wesnousky, S. G., Bormann, J. M., Kreemer C., Hammond W. C., Brune, J. N., 2012, Neotectonics, geodesy, and seismic hazard in the Northern Walker Lane of Western North America: Thirty kilometers of crustal shear and no strike-slip?: Earth and Planetary Science Letters, v. 329-330, p. 133–140

Wood, H. O. and Neumann F., 1931, Modified Mercalli Intensity Scale of 1931: Bulletin of the Seismological Society of America, v. 21, p. 277-283

Workman, J.B., Lundstrom, S.C., Blakely, R.J., and Dixon, G.L., 2008, Geologic map of the Hidden Hills Ranch Quadrangle, Clark County, Nevada: U.S. Geological Survey Scientific Investigations Map 3033, 1 sheet, scale 1:24,000

Youd, T., L., 1973, Liquefaction, flow and associated ground failure; United States Geological Survey Circular 688, 12 pp.

Zhang, P., Ellis M.A., Slemmons , D.B., Mao, F., 1990, Right-lateral displacements associated with prehistoric earthquakes and Holocene slip rate along the southern Panamint Valley fault zone: implications for southern Basin and Range tectonics: Journal of Geophysical Research, v. 95, p. 4857-4872, doi:10.1029/JB095iB04p04857

VITA

Graduate College
University of Nevada, Las Vegas

Jonathan Andrew Carter

Degrees:
    Bachelor of Science, Geology 2009
    University of Nevada, Las Vegas

Thesis Title: Microstructural Paleoseismic study of the Stewart Valley and
    Northern Pahrump segments of the Stateline Fault System, Nevada.

Thesis Examination Committee:
    Chairperson, Wanda Taylor Ph.D.
    Committee Member, Michael Wells, Ph.D.
    Committee Member, Brenda Buck, Ph.D.
    Graduate Faculty Representative, Barbara Luke, Ph.D.